Triple oxygen isotope compositions of globally distributed soil carbonates record widespread evaporation of soil waters

Manuscript for submission to Geochimica et Cosmochimica Acta

Julia R. Kelson [a], Tyler E. Huth [a,b], Benjamin H. Passey [a], Naomi E. Levin [a], Sierra V. Petersen [a] Paolo Ballato [c], Emily J. Beverly [d], Daniel O. Breecker [e], Gregory D. Hoke [f], Adam M. Hudson [g], Haoyuan Ji [h], Alexis Licht [i], Erik Oerter [j], Jay Quade [k]

[a] *Department of Earth and Environmental Sciences, University of Michigan, Ann Arbor MI, 48109, USA*
[b] *Department of Earth and Planetary Sciences, Washington University in St. Louis, St. Louis, MO, 63130, USA*
[c] *Department of Science, Geological Sciences Section, University of Roma Tre, Rome, Italy*
[d] *Department of Earth and Atmospheric Sciences, University of Houston, Houston, Texas, 77204, USA*
[e] *Department of Geological Sciences, Jackson School of Geosciences, University of Texas at Austin,78712, USA*
[f] *Department of Earth and Environmental Sciences, Syracuse University, Syracuse, New York, 13244, USA*
[g] *US Geological Survey, Geosciences and Environmental Change Science Center, Denver, Colorado 80225, USA*
[h] *Google LLC, Seattle, WA 98109*
[i] *Aix-Marseille Université, CNRS, IRD, INRAE, Collège de France, CEREGE, Aix-en-Provence, France*
[j] *Nuclear and Chemical Sciences Division, Lawrence Livermore National Laboratory, Livermore CA, 94550, USA*
[k] *Department of Geosciences, University of Arizona, Tucson, AZ 85721, USA.*

Abstract

The stable isotopic composition of pedogenic carbonates is central to many studies of past climate and topography, providing a basis for our understanding of Earth's terrestrial history. A core assumption of many applications of oxygen isotope values ($\delta^{18}O$) of pedogenic carbonate is that they reflect the $\delta^{18}O$ value of precipitation (rain/snow). This assumption is violated if soil carbonates form in evaporated soil waters. In this work, we develop a means to identify evaporation in ancient soils using the triple oxygen isotope composition (^{16}O-^{17}O-^{18}O) of pedogenic carbonates. Both theoretical predictions of isotope kinetics during evaporation and

studies of triple oxygen isotopes in other geological materials show that the deviation in the relationship between $\delta^{17}O$ and $\delta^{18}O$ from a reference line, evaluated using the parameter $\Delta'^{17}O$, is sensitive to evaporation. As a first step in developing the use of $\Delta'^{17}O$ in ancient pedogenic carbonates, we report $\Delta'^{17}O$ values from 47 near-modern pedogenic carbonate samples from globally distributed environments that vary in aridity (hyper-arid to humid). The $\Delta'^{17}O$ values of pedogenic carbonate range from -154 to -60 per meg (as $CaCO_3$, measured via O_2, VSMOW-SLAP), corresponding to calculated soil water values of -66 to +27 per meg (VSMOW-SLAP) (using a carbonate-water triple oxygen isotope fractionation exponent of 0.5250 and clumped isotope-derived carbonate growth temperatures). The $\Delta'^{17}O$ values indicate that evaporative modification of soil water from which pedogenic carbonate forms is common, especially in arid environments. Arid environments host pedogenic carbonates formed from soil waters ranging from highly to minimally evaporated, while humid environments host pedogenic carbonates formed from waters that are only minimally evaporated. The variability in $\Delta'^{17}O$ within environments classified by the same aridity may relate to the fact that pedogenic carbonates record soil conditions only during times of carbonate mineralization, which may deviate from annual conditions. Thus, $\Delta'^{17}O$ may be useful in understanding the specific circumstances of pedogenic carbonate formation but may not provide incontrovertible evidence of the magnitude of environmental aridity. Evaporative modification of $\delta^{18}O$ values of pedogenic carbonates can be detected with $\Delta'^{17}O$, thereby improving estimates of $\delta^{18}O$ of unevaporated waters. Our data show that evaporation must be (re)considered for all paleoclimate inferences based on the $\delta^{18}O$ of pedogenic carbonate. The addition of $\Delta'^{17}O$ will re-energize paleoclimate studies that use (or have avoided using) $\delta^{18}O$ of pedogenic carbonate.

Key Words

soils; triple oxygen isotopes; clumped isotopes; terrestrial paleoclimatology; evaporation

1. Introduction

The relative abundance of ^{18}O and ^{16}O in pedogenic carbonates ($\delta^{18}O_{carb}$) has been a foundational tool used in major discoveries of Earth history events, such as uplift of the Andes and Himalaya mountains, fluctuations in air and soil temperatures, and changes in water balance amidst grassland expansion in North America and Africa (Cerling, 1992; Cole and Monger, 1994; Fox and Koch, 2003; Garzione et al., 2008; Levin et al., 2011; Eagle et al., 2013; Snell et al., 2013; Rech et al., 2019). While variations in $\delta^{18}O_{carb}$ have allowed workers to discover major environmental changes, the precise driving processes are difficult to constrain without additional information because $\delta^{18}O_{carb}$ is sensitive to multiple environmental factors. The two primary factors that control $\delta^{18}O_{carb}$ are carbonate growth temperature and the $\delta^{18}O$ value of soil water, which varies with evaporation and/or with changes in the $\delta^{18}O$ value of meteoric waters that recharge the soil (e.g., due to precipitation seasonality, moisture source, or infiltration paths). With the development of carbonate clumped isotope thermometry, we can now constrain carbonate growth temperatures and calculate the $\delta^{18}O$ value of parent soil water (Quade et al., 2007a; Eiler, 2007; Huntington and Petersen, 2023). This leaves workers who wish to interpret $\delta^{18}O$ of soil water reconstructed from $\delta^{18}O_{carb}$ with a quandary: when has $\delta^{18}O$ been modified by evaporation, and when can it be trusted as a record of primary meteoric waters? And a corollary: does evaporative enrichment in ^{18}O indicate arid conditions?

In many applications, $\delta^{18}O_{carb}$ is used primarily to infer $\delta^{18}O$ values of meteoric waters and to investigate hydrologic processes including the seasonal balance of precipitation (Smith et

al., 1993; Oerter et al., 2016; Kukla et al., 2022), local temperature of rainfall (Nordt et al., 2003; Fricke and Wing, 2004), water-energy balance (Kukla et al., 2019; van Dijk et al., 2020), regional circulation patterns including monsoon intensity, continentality, and moisture recycling (Liu et al., 1996; Monger et al., 1998; Fricke et al., 2010; Winnick et al., 2013, 2014; Methner et al., 2016; Licht et al., 2017; Caves Rugenstein and Chamberlain, 2018), and paleoelevations (Garzione et al., 2008; Hoke et al., 2009, 2014; Fan et al., 2011; Chamberlain et al., 2012; Mulch et al., 2015; Song et al., 2018). These applications assume that $\delta^{18}O_{carb}$ has been minimally affected by evaporation, especially at depths > 40 cm below the surface, but this is a known simplification that is at odds with an abundance of isotopic data showing evaporatively enriched pore waters in deep and shallow vadose zones (Barnes and Allison, 1983; Allison et al., 1983; Quade et al., 1989; Wang et al., 1996; Liu et al., 1996; Hsieh et al., 1998; Monger et al., 1998; DePaolo et al., 2004; Brooks et al., 2010; Evaristo et al., 2015; Oerter and Amundson, 2016). In another class of applications, workers interpret increases in $\delta^{18}O_{carb}$ as primarily or possibly reflecting evaporation, which is often linked to changes in environmental aridity (Amundson and Lund, 1987; Amundson et al., 1989, 1994; Kleinert and Strecker, 2001; Levin et al., 2004, 2011; Fox and Koch, 2004; DeCelles et al., 2007; Zhou and Chafetz, 2010; Chamberlain et al., 2014; Ji et al., 2017; Kelson et al., 2018; Rech et al., 2019; Broz et al., 2021). These varied uses of $\delta^{18}O_{carb}$ demonstrate the need for a tool that can disentangle evaporation in soil pore waters from the various drivers of change in $\delta^{18}O$ of meteoric water. We also need to understand if the magnitude of evaporation in soil waters reconstructed from carbonates can be used to assess aridity in the geologic record.

Ecohydrologists have used oxygen and hydrogen isotopes ($\delta^{18}O$, $\delta^{2}H$) to show that shallow (<30 cm) soil water worldwide is often evaporated, and that in arid and semi-arid

105 climates the depth of evaporated soil waters may be deeper (Sprenger et al., 2016). Evaporated
106 soil water is isotopically distinct from local meteoric waters such as rain, river, and ground water
107 (Brooks et al., 2010; Evaristo et al., 2015; Bowen et al., 2018). Though the potential for
108 evaporative effects on $\delta^{18}O$ of soil carbonate was recognized early in the field (Quade et al.,
109 1989; Cerling and Quade, 1993), it remains unclear the extent to which carbonate-parent soil
110 water has an evaporative signature, and how its isotopic composition ultimately relates to that of
111 meteoric waters (Kelson et al., 2020). This uncertainty persists in part because of spatial and
112 temporal heterogeneity in the isotopic composition of soil water that results from percolation of
113 isotopically variant input water, evaporation, mixing with antecedent pore water, redistribution
114 by vegetation (Gazis and Feng, 2004; Sprenger et al., 2016; Benettin et al., 2018), and the
115 possibility of multiple pools of water within soil pores (Brooks et al., 2010; Sprenger and Allen,
116 2020). Furthermore, the most common carbonate minerals (calcite, aragonite) do not contain
117 structural hydrogen, and so carbonate minerals cannot be directly compared to $\delta^{18}O$-$\delta^{2}H$
118 meteoric water lines. Thus, even with $\delta^{18}O_{water}$ and $\delta^{18}O_{carb}$ measurements in modern soils, it is
119 difficult to infer the source and the evaporative trajectory of the soil-carbonate parent waters
120 (Breecker et al., 2009; Takeuchi et al., 2009; Oerter and Amundson, 2016; Havranek et al., 2020;
121 Beverly et al., 2021).
122 Recent work has shown that the relative abundances of the three isotopes of oxygen (^{16}O,
123 ^{17}O, ^{18}O) in water are sensitive to evaporation (Barkan and Luz, 2007; Luz and Barkan, 2010;
124 Surma et al., 2015) and that this signal is preserved and can be measured in carbonates (Passey et
125 al., 2014; Barkan et al., 2015; Fosu et al., 2020; Wostbrock et al., 2020b). Evaporation is a
126 kinetic process that causes the slope between $\delta'^{17}O$ and $\delta'^{18}O$ to deviate from a reference slope
127 (here $\lambda_{ref} = 0.528$) that approximates the relationship observed in meteoric waters, evaluated with

the term $\Delta'^{17}O$ (Figure 1) (Barkan and Luz, 2007) (notation defined in 2.1). $\Delta'^{17}O$ has been shown to be sensitive to evaporation in meteoric waters (Landais et al., 2010; Luz and Barkan, 2010; Li et al., 2015; Evans et al., 2018; Surma et al., 2018, 2021; Aron et al., 2021a, b, 2023; Giménez et al., 2021; Voigt et al., 2021; Xia, 2023) and leaf waters (Landais et al., 2006; Li et al., 2017). Authigenic minerals inherit their parent water's evaporative signature, including in $\Delta'^{17}O$ values, as measured in silicates (Ibarra et al., 2021), lake carbonates (Passey and Ji, 2019; Katz et al., 2023), gypsum hydration waters (Herwartz et al., 2017; Gázquez et al., 2018), soil phytoliths (Alexandre et al., 2018; Voigt et al., 2023), and tooth enamel (Pack et al., 2013; Passey et al., 2014; Lehmann et al., 2022). Because of its sensitivity to evaporation, $\Delta'^{17}O$ has been proposed to be a proxy for environmental aridity in soil phytoliths, mammal tooth enamel, and pedogenic carbonates (Alexandre et al., 2018; Beverly et al., 2021; Lehmann et al., 2022). Pedogenic carbonates are a logical target for this emerging technique given that they form in the shallow vadose zone waters that are vulnerable to evaporation, as initially discussed in Passey et al. (2014). In a regionally focused study, Beverly et al. (2021) showed that the $\Delta'^{17}O$ of Holocene pedogenic carbonates related to aridity in Tanzania, suggesting that $\Delta'^{17}O$ relates to the magnitude of local evaporation. Although these initial findings are promising, they need to be validated across diverse ecosystems before $\Delta'^{17}O$ of pedogenic carbonates can be used in paleoclimate applications to detect evaporation and/or to reconstruct aridity.

The first purpose of this study is to evaluate the prevalence of evaporation in soil waters from which pedogenic carbonates form. This objective will test the often-made assumption that $\delta^{18}O_{carb}$ primarily reflects $\delta^{18}O$ of minimally evaporated meteoric waters (see citations above). The second purpose of this study is to determine if $\Delta'^{17}O$ in pedogenic carbonates can be used to indicate paleo-aridity. To meet these objectives, we measure $\Delta'^{17}O$ of pedogenic carbonates from

varying climate regimes. We also estimate carbonate growth temperatures, using carbonate clumped isotope thermometry (Δ_{47}) where possible, which we use to calculate $\delta^{18}O$ and $\Delta'^{17}O$ of parent soil water ($\delta^{18}O_{rsw}$ and $\Delta'^{17}O_{rsw}$). We assess evaporation by comparing the $\delta^{18}O$ and $\Delta'^{17}O$ of reconstructed soil water to that of global meteoric waters. We predict the effects of evaporation on pedogenic carbonate $\Delta'^{17}O$ values with a simple mathematical model (Barnes and Allison; 1983). Finally, we use geographically related samples as a basis to suggest how $\Delta'^{17}O$ can be most useful for paleoclimate workers to evaluate the importance of evaporation in $\delta^{18}O$ values and improve estimates of pristine $\delta^{18}O$ of recharge waters.

2. Site Descriptions and Methods

2.1 Triple oxygen isotope notation

Mass-dependent fractionation for triple oxygen isotope systems is described with a power law relationship that relates the fractionation factor (α) between two phases (A and B) with an exponent (θ):

$$^{17}\alpha_{(A-B)} = \left(^{18}\alpha_{(A-B)}\right)^{\theta} \quad (1)$$

The exponent θ denotes fractionation that occurs from a single process whose value is derived from experiments or theory. Equilibrium exchange between water vapor and liquid water is described by $\theta_{eq} = 0.529$ (Young et al., 2002; Barkan and Luz, 2005). Evaporation is a kinetic process that involves the diffusion of water vapor through air and is described with $\theta_{diff} = 0.5185$ (Barkan and Luz, 2007). The difference between θ_{eq} and θ_{diff} is the basis for using triple oxygen isotopes to detect evaporation (Figure 1A). The notation λ is often used in place of θ in Equation 1 to describe empirically observed triple oxygen isotope relationships that might combine

multiple processes (i.e., evaporation in natural soils that combines equilibrium and diffusive fractionation, or λ_{soil}). For practicality of visualizing and working with triple oxygen isotope data, the power law relationship in Equation 1 can be linearized using δ' notation (Miller, 2002):

$$\delta' = \ln(R_{SA}/R_{ST}) \quad (2)$$

And then the $\Delta'^{17}O$ parameter can defined as the deviation from an empirically derived reference line of meteoric waters (λ_{ref}):

$$\Delta'^{17}O = \delta'^{17}O - \lambda_{ref} * \delta'^{18}O \quad (3)$$

We use the reference slope (λ_{ref}) of 0.528, a value that was established to describe global meteoric waters (Luz and Barkan, 2010; Aron et al., 2021a) and has been adopted in the reporting $\Delta'^{17}O$ of geological materials that track the hydrosphere (Evans et al., 2018; e.g., Sharp et al., 2018; Passey and Ji, 2019; Sengupta et al., 2020; Ibarra et al., 2021; Sharp and Wostbrock, 2021; Huth et al., 2022; Kelson et al., 2022; Lehmann et al., 2022). The parameters θ and λ are used to describe slopes of linear regressions where $\delta'^{18}O$ and $\delta'^{17}O$ are the predicted and response variables, respectively (Figure 1A), and generally have a physical basis (i.e., evaporation). We also use apparent trends in $\delta'^{18}O$-$\Delta'^{17}O$ space for ease of plotting and conceptualization (Figure 1B; Figure 2C).

2.2 Theoretical prediction of triple oxygen isotopes in soil water resulting from evaporation

We modified an existing, relatively simple, mathematical model for the distribution of $H_2{}^{18}O$ and HDO in soil water (Barnes and Allison, 1983) to predict the distribution of $H_2{}^{17}O$ in soil water resulting from evaporation in a soil profile in quasi-steady state conditions. The goal was to provide a basic framework for understanding the influence of evaporation on $\Delta'^{17}O$ values of soil water, in terms of direction and magnitude, relationship with $\delta^{18}O$, and depth distributions

194 (Supplementary Text Section 1). We modeled evaporation as diffusive transport of water vapor
195 from the soil water surface (e.g., Criss, 1999). The soil profile was modeled with two zones: a
196 shallow 'dry' zone (vapor transport only, relative humidity varies from 100% to the value of the
197 overlying atmosphere) that is above a 'wet' zone (dominated by liquid transport, with relative
198 humidity of 100%). The boundary between these zones was termed the evaporation front (z_{ef}).
199 Kinetic isotope fractionation due to evaporation occurs at the evaporation front, and liquid water
200 influenced by evaporation diffuses downward into the 'wet' zone. There is upward advection of
201 unevaporated water from the water table in the 'wet' zone. The model equations can be found in
202 Barnes and Allison (1983), Fischer-Femal and Bowen (2021), and in Supplementary Text
203 Section 1. We built on the existing model of $\delta^{18}O$ and $\delta^{2}H$ by calculating $\delta^{17}O$, and $\Delta'^{17}O$ via the
204 triple oxygen isotope exponents for equilibrium and diffusive processes ($\theta_{eq} = 0.529$, $\theta_{diff} =$
205 0.5185) (Figure 2) (Barkan and Luz, 2007). To explore the scale and magnitude of isotopic
206 changes caused by evaporation, we varied the physical and isotopic parameters in the model
207 (Supplementary Text Section 1, Figures S1-S4).
208
209 *2.3 Site and sample selection, age control, and climate data*
210 To maximize our potential to observe a large range in evaporative states and in $\Delta'^{17}O$
211 values, we targeted soil carbonates from sites that vary in climate regime, including variation in
212 aridity (hyper-arid to subhumid), elevations, and seasonal temperatures (Table 1) (Figure 3).
213 Vegetation cover varies across the sites, but most are shrub- or grassland (or a mix), and some
214 have very sparse vegetation. Very few of the sites have trees (only the sites in Texas and
215 Myanmar could be considered forested) (Supplementary Text Section 2). Most of the soil
216 carbonate samples were originally collected for other studies (e.g., typically focusing on $\delta^{18}O$ or

Δ_{47}); some were newly collected (Table 1; Supplementary Text Section 2). The pedogenic carbonate morphologies include rinds, diffuse carbonate, and nodules (see Figures S5–S11 for site pictures). While we have sought to sample stable geomorphic surfaces, for some soil sites the depth of sampling may not be equivalent to the depth of carbonate formation because land surfaces can undergo erosion and accumulation, resulting in generations of pedogenic overprinting (e.g., Deutz et al., 2002). We sampled and analyzed pedogenic carbonate at multiple depths in a soil profile where possible to test if evaporative effects are more pronounced near the surface.

One assumption in this work (and previous studies focusing on $\delta^{18}O$, $\delta^{13}C$, and Δ_{47}) is that modern climate data can be used to contextualize the conditions of pedogenic carbonate formation in surface (i.e., not buried or relict) soils (e.g., Quade et al., 2007b, 2013; Breecker et al., 2009; Peters et al., 2013; Burgener et al., 2016; Gallagher and Sheldon, 2016; Oerter and Amundson, 2016; Ringham et al., 2016; Gallagher et al., 2019; Huth et al., 2019; Beverly et al., 2021). To minimize inaccuracies introduced because of this assumption, we targeted pedogenic carbonates that are near-modern (i.e., Holocene, though some are late Pleistocene). Some pedogenic carbonate samples have age controls based on dating of the geomorphic surface and/or the carbonate itself; where age constraints did not exist we sampled carbonates that were likely to be young based on incipient soil and carbonate development (Gile et al., 1966) and geomorphic context (Supplementary Text Section 2). To classify the moisture availability at each site, we extracted Aridity Index (AI), the ratio between mean annual precipitation and potential evapotranspiration, from World Clim 2 and Version 3 of the Global Aridity Index and Potential Evapotranspiration Database (30 arc-second grid resolution) (Fick and Hijmans, 2017; Zomer et al., 2022). This is an updated version of the Global AI database compared to what was used in

Beverly et al. (2021), so the absolute values differ (but patterns remain) compared to what was reported in that publication. To test if depletion in $\Delta'^{17}O_{rsw}$ is accompanied by enrichment in $\delta^{18}O_{rsw}$ relative to $\delta^{18}O$ of recharge waters, we needed an estimate of $\delta^{18}O$ of recharge waters. We turned to estimates of amount-weighted mean annual $\delta^{18}O$ of precipitation ($\delta^{18}O_{ann}$) at each site, while acknowledging that this method overlooks potential seasonal bias in recharge and complexities in soil water hydrology (Gazis and Feng, 2004; Sprenger et al., 2016). We also considered the mean $\delta^{18}O$ value of monthly precipitation during the estimated season of carbonate formation, in accordance with evidence that pedogenic carbonate $\delta^{18}O$ is seasonally biased (Hough et al., 2014; Kelson et al., 2020) (Supplementary Text Section 3). We extracted estimates of $\delta^{18}O$ values of precipitation (monthly and $\delta^{18}O_{ann}$) from the Oxygen Isotopes of Precipitation Calculator (OIPC) (Bowen and Revenaugh, 2003) (estimates of $\Delta'^{17}O$ precipitation are not currently available). For the samples from Ethiopia (Table 1), the range of precipitation $\delta^{18}O$ and $\delta^{18}O_{ann}$ are derived from the long-term, amount-weighted mean of rainfall at Addis Ababa (-1.3 ± 2.3 ‰) from the Global Network of Isotopes in Precipitation (GNIP) (Rozanski et al. 1993; IAEA 2013) instead of the OIPC value because of known inaccuracies in the OIPC in that region (Levin et al., 2009; Kebede et al., 2021) (OIPC-derived $\delta^{18}O_{ann}$ is + 3.4 ‰). We also employed GNIP data (1982-1984) for the NAC soil site at the Ñacuñán Biosphere Reserve because of their collocation, although we note that at this location the difference between the OIPC and GNIP values of $\delta^{18}O_{ann}$ is minor (0.3 ‰). At each site, we estimated $\Delta'^{17}O_{mw}$ using the mean of $\Delta'^{17}O$ values of global, unevaporated meteoric waters (Aron et al., 2021a) within the range of precipitation $\delta^{18}O$ values.

2.4 Analytical Methods

263

264 *2.4.1 Triple Oxygen Isotope Analytical and Normalization Methods*

265 We consider $\Delta'^{17}O$ values measured in pedogenic carbonate that are new to this study (21
266 samples), values from Beverly et al. (2021) (14 samples), values from Passey et al. (2014) (7
267 samples), and values from Ji (2016) (5 samples). We describe the methods for measuring $\Delta'^{17}O$
268 values of the samples new to this study and then discuss normalization steps taken to make
269 previously published data comparable to the newly generated data.

270 The $\Delta'^{17}O$ measurements of carbonate new to this study were made at the University of
271 Michigan (UM) following the acid digestion-reduction-fluorination method described in detail in
272 Passey et al. (2014) and Passey and Levin (2021). In brief, we converted the carbonate samples
273 ($CaCO_3$) to O_2 gas for analysis on a mass spectrometer to avoid a mass interference between ^{13}C
274 and ^{17}O in CO_2. We digested the carbonates in a common phosphoric acid bath held at 90 °C to
275 yield CO_2 gas. The resulting CO_2 was purified then reduced with hydrogen gas, aided by an iron
276 catalyst to produce H_2O. The resulting H_2O was fluorinated in a cobalt fluoride (III) reactor held
277 at 360 °C to produce O_2 (Barkan and Luz, 2005). We measured masses 32–36 of O_2 on a Nu
278 Perspective isotope ratio mass spectrometer. We observed a memory effect within the cobalt
279 fluoride (III) reactor that is minimized by analyzing samples in isotopic order (Huth et al., 2022).
280 We typically measure the $\delta^{18}O$ value of a sample as CO_2 with a mass spectrometer before
281 measuring $\Delta'^{17}O$. Sample analyses with $\delta^{18}O$ values that were >5 ‰ different from the previous
282 sample were removed from the dataset.

283 We defined analytical sessions based on when we refreshed the CoF_3 material in the
284 fluorination reactor or performed other maintenance (e.g., changing the filament of the mass
285 spectrometer, power outages). In each analytical session, we measured both water and carbonate

standards. Water standards, VSMOW2 and SLAP2, provided the normalization basis for the VSMOW2-SLAP2 reference frame (Schoenemann et al., 2013) (henceforth abbreviated as VSMOW-SLAP). Water standards were analyzed using the same fluorination and vacuum line as the carbonate-derived waters. Multiple analyses (2 to 4 replicates) of VSMOW2 and SLAP2 were performed at the start, middle and end of each analytical session (see supplementary tables for run order and standard values). International carbonate standards (NBS-18, NBS-19, IAEA 603, IAEA C1) and an internal carbonate standard (102-GC-AZ01) were analyzed along with unknowns. We corrected the O_2-derived delta values of sample gas to carbonate mineral delta values via the Wostbrock et al. (2020b) values of international standards, using empirically derived fractionation factors which include all fractionations imparted in our analytical method (acid digestion, reduction, and fluorination) (Passey et al., 2014; Huth et al., 2022). The fractionation factors were calculated using the carbonate mineral value of IAEA-603 derived by Wostbrock et al (2020b) via carbonate fluorination ($\delta^{17}O$ = 14.831 ± 0.007 ‰ VSMOW-SLAP, $\delta^{18}O$ = 28.470 ‰ VSMOW-SLAP, $\Delta'^{17}O$ = -100 ± 7 per meg VSMOW-SLAP) and the long term average of IAEA-603 measured in our laboratory ($\delta^{18}O$ = 36.233 ± 1.224 ‰ VSMOW-SLAP, $\Delta'^{17}O$ = -146 ± 15 per meg VSMOW-SLAP) (described in Huth et al., 2022). The UM fractionation factors are ${}^{17}\alpha_{mineral-90°C\ acid,O_2}$ = 0.9957458 and ${}^{18}\alpha_{mineral-90°C\ acid,O_2}$ = 0.9918723 ($\theta_{mineral-90°C\ acid,O_2}$= 0.5224) (Huth et al., 2022). Finally, we corrected the $\Delta'^{17}O$ mineral values for drift on a session-by-session basis using the average mineral $\Delta'^{17}O$ values of IAEA-603 and IAEA-C1 (-100 per meg, by definition; IAEA 603 and IAEA C1 are isotopically identical, Huth et al., [2022]). This session-specific drift correction is usually less than ± 12 per meg. $\delta^{17}O$ values are re-calculated based on the corrected $\Delta'^{17}O$ values.

The long-term standard deviation (S.D.) of $\Delta'^{17}O$ of 102-GC-AZ01 (13 per meg, n = 95 replicates) is considered our minimum external error and is used to calculate standard error in place of 1 S.D. of sample replicates when the S.D. of sample replicates is smaller. We observe typical external reproducibility (1 S.D.) of 2 to 20 per meg for replicate analyses of a sample. Measurements are replicated 1-4 times for individual samples.

To compare our $\Delta'^{17}O$ data to previously published soil carbonate $\Delta'^{17}O$ data from Beverly et al. (2021), Ji (2016), and Passey et al. (2014), we adjusted the previously reported values so that they are consistent with the normalization schemes used in this study. The soil carbonate $\Delta'^{17}O$ data of Beverly et al. (2021) were generated in the same laboratory following the same preparation and analytical methods as the data new to this study. However, the Beverly et al. (2021) data were originally presented as O_2 values. We calculated the mineral values for those samples using the UM-specific empirically derived fractionation factors as described above. Additionally, we screened 6 of the 39 original analyses for the $\delta^{18}O$ memory effect (this memory effect had not yet been described in the UM laboratory at the time of that study). These renormalization efforts do not affect the major findings of that study.

We also re-report $\Delta'^{17}O$ values of soil carbonates that were produced at Johns Hopkins University (JHU), using a similar reduction - fluorination analytical procedure as employed at the UM (data from Ji, 2016 and Passey et al., 2014). These $\Delta'^{17}O$ data were originally reported as O_2 gas values. We normalized the JHU data to carbonate mineral values (Wostbrock et al., 2020b; Sharp and Wostbrock, 2021) using empirically derived fractionation factors specific to JHU. The mineral-(90°C acid-O_2) fractionation factors were calculated using the mineral value of NBS-19 from Wostbrock et al. (2020b) ($\delta^{17}O$ = 14.923 ± 0.010 ‰ VSMOW-SLAP, $\delta^{18}O$ = 28.650 ‰ VSMOW-SLAP, $\Delta'^{17}O$ = -102 ± 10 per meg VSMOW-SLAP) and the long term

average NBS-19 value from JHU (excluding two problematic sessions, n = 43, $\delta^{18}O$ = 36.998 ± 0.6930‰ VSMOW-SLAP, $\Delta'^{17}O$ = -139 ± 10 per meg VSMOW-SLAP). The JHU fractionation factors are ${}^{17}\alpha_{mineral-90°C\ acid,O_2}$ = 0.9957782 and ${}^{18}\alpha_{mineral-90°C\ acid,O_2}$ = 0.9919498 ($\theta_{mineral-90°C\ acid,O_2}$ = 0.5234). Finally, we applied a session-specific drift correction to the $\Delta'^{17}O$ mineral values using the mineral value of NBS-19 defined by Wostbrock et al. (2020b) (-102 per meg, VSMOW-SLAP). For sessions including JHU analytical numbers 1104-1208 (sample IDs GON07-4.6-02; GON07-4.7-1; CA08-005-1; ET05-AWSH-48-1), NBS-19 was not analyzed, so we relied on a tank CO_2 standard to perform a final drift correction. The "mineral" value of tank CO_2 is defined via analysis in other sessions against NBS-19 ($\Delta'^{17}O$ value = -0.077 ‰).

2.4.2 Clumped Isotope Analytical and Normalization Methods (Δ_{47}, $\delta^{13}C$, $\delta^{18}O$)

We present clumped isotope (Δ_{47}) data for 40 of the 47 soil carbonate samples considered in this study. $\delta^{13}C$ and $\delta^{18}O$ data are generated simultaneously as a part of the Δ_{47} measurement. Some data were previously published, and some are new to this work (Table 1, Table 3). For the samples with clumped isotope data that have been reported in previous publications, we use the Δ_{47} and $T\Delta_{47}$ values as originally reported. All Δ_{47} data are reported relative to 25 °C acid digestion (Table 3). There are minor differences in the acid fractionation factor used (i.e., Beverly et al., (2021) used 0.082 from Defliese et al., (2015); most others used 0.088 of Petersen et al., (2019)), and minor differences in the reference frames (i.e., some data pre-date the ICDES and the CDES) (Table 3). The Δ_{47} data that are new to this study were generated at UM in two different laboratories (Table 3).

Clumped isotope data for six of the samples from this study were generated at the Stable and Clumped Isotope for Paleoclimate and Paleoceanography (SCIPP) Laboratory at UM in July-December of 2020 (Table 3) (including the two samples of Licht et al., (2022)). Carbonate samples (4–7 mg) were digested in phosphoric acid held at 70 °C in individual vials and purified using a NuCarb automated sample preparation device (Jones et al., 2022; O'Hora et al., 2022). Resulting CO_2 gas was analyzed on a Nu Perspective mass spectrometer. Raw Δ_{47} values were calculated with the ^{17}O correction parameters of Brand et al. (2010) (Schauer et al., 2016; Daëron et al., 2016). These Δ_{47} values were standardized using an equal proportion of standards ETH 1-4, by assigning the community-defined InterCarb (ICDES90) values (Bernasconi et al., 2021) which inherently include an acid fractionation factor of 0.088 ‰ to account for the difference in Δ_{47} between CO_2 reacted at 25 °C and 90 °C (Petersen et al., 2019). Temperatures were calculated using the calibration of Anderson et al. (2021), which is reported in the ICDES90 reference frame. The error reported for sample Δ_{47} values is calculated as standard error of 2-4 measured replicates. The standard deviation used is the larger value of either the standard deviation of Carrara Marble in the session (0.013 ‰, n = 23) or the standard deviation of sample replicate values. Finally, we report the sample values in the ICDES25 reference frame (adjust the values by an acid fractionation factor of 0.088 from Petersen et al. [2019]) to present the data in Table 3 alongside previously published data that had been reported relative to digestion at 25 °C.

Clumped isotope data for four of the samples from this study were generated at the Isotopologue Paleosciences Laboratory (IPL) at UM (Table 3). Carbonate samples (6–8 mg of carbonate equivalent) were digested in a common phosphoric acid bath held at 90°C. The resulting CO_2 was cryogenically separated from water and then carried with helium through a Poropak Q trap held at -20 °C in a bespoke extraction line that is directly connected to a Nu

Perspective. Raw Δ_{47} values were calculated with the ^{17}O correction parameters of Brand et al. (2010) (Schauer et al., 2016; Daëron et al., 2016) and were normalized with a hybrid gas and carbonate standards approach similar to the InterCarb (ICDES) framework (Bernasconi et al., 2021). Equilibrated and heated gases (30°C and 1000 °C) (known values from Petersen et al., 2019) were combined with carbonate standards ETH1-3 (accepted values from Bernasconi et al., 2021) to correct the sample Δ_{47} values for compositional nonlinearity and project them into the ICDES-90 reference frame, using the single equation formulation of Daeron et al. (2016). Temperatures were calculated using the calibration of Anderson et al., (2021). Finally, we correct the samples to relative to acid digestion at 25 °C (i.e., place them into the ICDES25 reference frame) using an acid fractionation factor of 0.088 from Petersen et al. [2019]). This allows us to present the data alongside previously published data that had been reported relative to digestion at 25 °C (Table 3).

2.4.3 Reconstructing soil waters ($\delta^{18}O_{rsw}$ and $\Delta'^{17}O_{rsw}$) from carbonates ($\delta^{18}O_{carb}$, $\Delta'^{17}O_{carb}$, Δ_{47})

We calculate the reconstructed soil water values ($\delta^{18}O_{rsw}$ and $\Delta'^{17}O_{rsw}$) so that we can compare the carbonate-generated isotope data directly to isotopic compositions of meteoric water. We calculated $\delta^{18}O_{rsw}$ and $\Delta'^{17}O_{rsw}$ using empirically derived carbonate-water fractionation factors for $\delta^{18}O_{sw}$ (Kim and O'Neil, 1997) and λ_{cc-w} :

$$1000ln^{18}\alpha_{cc-w} = 18030/T - 32.42 \quad (4)$$

$$^{17}\alpha = (^{18}\alpha)^{\lambda_{cc-w}} \quad (5)$$

Using the expression for $^{18}\alpha_{cc-w}$ of Wostbrock et al. (2020a) rather than Kim and O'Neil (1997) results in $\delta^{18}O_{rsw}$ values that differ by 1 ‰ and $\Delta'^{17}O_{rsw}$ values that differ by ~2–5 per meg (Figure S12) (a magnitude of difference that is not relevant to our interpretations). We use

397 λ_{cc-w} = 0.5250 ±0.0021 that was established empirically in our laboratory through analysis of
398 synthetic and natural calcites and their parent waters (Huth et al., 2022; Kelson et al., 2022)
399 (Figure S17). Although most studies find a similar λ_{cc-w} value (range from 0.5231 to 0.5254),
400 the discrepancies in the fourth decimal place will change the reconstructed $\Delta'^{17}O$ water values on
401 the order of 10 per meg (Bergel et al., 2020; Voarintsoa et al., 2020; Wostbrock et al., 2020; see
402 Figure 5 of Huth et al. [2022]). The discrepancies in λ_{cc-w} are poorly understood; we rely on our
403 in-house λ_{cc-w} value because the empirically derived λ_{cc-w} values may incorporate fractionation
404 inherent to each analytical procedure. The $\Delta'^{17}O_{rsw}$ values could be revised in the future as
405 λ_{cc-w} values become better constrained.
406 We used the $\delta^{18}O_{carb}$ values obtained by mass spectrometry via analysis as CO_2 (usually
407 simultaneous with Δ_{47} analyses) (Table 3) to calculate $\delta^{18}O_{rsw}$ because these values are more
408 accurate and precise than the $\delta^{18}O$ values obtained via O_2-based analysis. The $\delta^{18}O_{carb}$ values
409 measured via O_2 as part of the $\Delta'^{17}O_{carb}$ measurement vs. via CO_2 as part of the Δ_{47} measurement
410 typically agree within 1 ‰, though there are discrepancies greater than 2 ‰ for eight of the
411 samples (19ND04 and PDJ 4055 115a that are new to this paper, 18-SS-236A-C, 18-SS-69A, 18-
412 SS-79A, GON07 samples, CA08-005-1, and BUR-MH-30Buff in previously reported samples).
413 Some of this discrepancy could be natural heterogeneity in soil carbonates; some could be due to
414 fractionation during the reduction-fluorination preparation steps (Passey et al., 2014). Where
415 possible, a clumped isotope temperature was used to constrain the growth temperature to
416 calculate α^{18}. For the Fish Lake Valley sites that do not have Δ_{47} data, we use spring and summer
417 average soil temperatures measured at 100 cm to approximate carbonate formation temperatures
418 (Oerter and Amundson, 2016). For the sites from Iran and New Mexico that do not have Δ_{47}
419 temperatures, we used a mean warm quarter air temperature from local meteorological stations

(Table 3) (Quade et al., 2013; Kelson et al., 2020; Fischer-Femal and Bowen, 2021). The cp3 site did not have sufficient material for Δ_{47} analysis, so we use the Δ_{47} temperature from the other Tibetan site, cp4 (Table 3). For the samples with Δ_{47} data, the uncertainty in mineral growth temperature is based on the external error in Δ_{47} and is typically less than 5 °C. For the samples without Δ_{47} data, the uncertainty in growth temperature is estimated using the difference between mean annual air temperature and mean warm quarter temperature. We estimated error in $\delta^{18}O_{rsw}$ and $\Delta'^{17}O_{rsw}$ by propagating error in growth temperature and external error in isotopic measurements with Monte Carlo resampling. The calculated $\delta^{18}O_{rsw}$ values are sensitive to growth temperature: a 5 °C temperature difference results in a ~1 ‰ difference in $\delta^{18}O_{rsw}$, which is large compared to the typical uncertainty of 0.1 ‰ in a $\delta^{18}O$ measurement but is the same order of magnitude as uncertainty associated with calibration of $^{18}\alpha$-temperature relationship. In comparison, $\Delta'^{17}O_{rsw}$ is less sensitive to growth temperature: a 5 °C temperature difference results in a ~3 per meg difference in $\Delta'^{17}O_{rsw}$, which is smaller than typical external error of 5 to 13 per meg in a $\Delta'^{17}O$ measurement.

3. Results

3.1 Predictions for $\delta^{18}O$ and $\delta^{17}O$ in a profile of soil water considering evaporation

The ^{17}O-modified Barnes and Allison (1983) model predicts that evaporation causes soil water to have higher $\delta^{18}O$ values and lower $\Delta'^{17}O$ values relative to input water (Figure 2). The maximum isotopic offset occurs at the evaporation front, the depth of which varies with relative humidity and evaporation rate (z_{ef}, typical depths of 0.1 to 0.3 m) (Figure 2; Figure S1). Above the z_{ef}, the isotopic composition of pore space water vapor is dominantly controlled by exchange

443 with the atmospheric water vapor, and below the z_{ef}, it is dominated by downward diffusion of
444 evaporatively-affected water. For the suite of model predictions with varying physical
445 parameters, we predicted maximum isotopic offsets that ranged from +3 to +40 ‰ in $\delta^{18}O$ and -
446 40 to -260 per meg in $\Delta'^{17}O$ (Figure S2). The maximum isotopic offset due to evaporation is
447 particularly sensitive to the humidity of the overlying atmosphere (Figure 2D). We calculate
448 linear regressions between $\delta'^{18}O$ and $\delta'^{17}O$ as predictor and response variables, respectively. The
449 resulting slopes (i.e., λ_{soil} values) range from 0.514 to 0.525 with a median of 0.517. There is
450 curvature in the relationship between $\delta'^{18}O$ and $\Delta'^{17}O$, but we describe a linear trend because it
451 can be compared to trends observed in natural systems where the low precision in $\Delta'^{17}O$
452 (typically ±10 per meg) masks curvature. The model-derived λ_{soil} values correspond to trends in
453 $\delta'^{18}O$ and $\Delta'^{17}O$ that range from -2 to -14 per meg/‰ with a median of -10.7 per meg/‰. The
454 corresponding slopes in $\delta^{18}O$-$\delta^{2}H$ space have a median value of 2.5.
455
456 *3.2 Stable isotope ($\delta^{13}C$, $\delta^{18}O$, $\Delta'^{17}O$, and Δ_{47}) results from natural pedogenic carbonates*
457 Tables 2 and 3 present stable isotope data from 47 individual pedogenic carbonates from
458 30 localities including 6 profiles, each with $\delta^{13}C$, $\delta^{18}O$ and $\Delta'^{17}O$ data. Of the 47 pedogenic
459 carbonates, 40 have accompanying Δ_{47} data. The range of $\delta^{13}C$ values is -13.9 to 2.1 ‰ (VPDB)
460 and the range of $\delta^{18}O_{carb}$ values is -17.0 to 4.3 ‰ (VPDB) (Tables 2 and 3). There is weak
461 covariation in $\delta^{13}C$ and $\delta^{18}O$ (Figure S13). The range of Δ_{47} values is 0.582 to 0.761 ‰
462 (ICDES25), corresponding to temperatures of 1 to 42 °C (Table 3).
463 The range of $\Delta'^{17}O_{carb}$ values is -154 to -60 per meg, corresponding to calculated $\Delta'^{17}O_{rsw}$
464 values of -66 to +27 per meg (λ_{cc-w} = 0.5250). Many, but not all, of the soil carbonates plot
465 outside of the $\delta^{18}O$-$\Delta'^{17}O$ population defined by global, un-evaporated meteoric waters (tap

466 water, springs, rivers or streams, precipitation, and groundwater, compiled in Aron et al. (2021))
467 (Figure 4). The $\Delta'^{17}O_{rsw}$ values determined from the pedogenic carbonates form a population
468 that is distinct from that of the global meteoric waters; the means of the populations of $\Delta'^{17}O$ of
469 reconstructed soil waters and of meteoric waters are statistically different according to a z-test
470 (p-value < 2.2e-16).

471 The data from the pedogenic carbonates show a wedge-like relationship between $\Delta'^{17}O$
472 and AI that does not change if $\Delta'^{17}O_{carb}$ or $\Delta'^{17}O_{rsw}$ values are considered (Figure 5) or if the
473 difference between $\Delta'^{17}O_{rsw}$ and $\Delta'^{17}O_{mw}$ is considered (Figure S14). We found a step-like pattern
474 where low $\Delta'^{17}O$ values are more common in more arid environments. The threshold occurs near
475 an AI value of 0.4: environments with AI values < 0.4 (hyper-arid to semi-arid environments)
476 have $\Delta'^{17}O_{carb}$ values that range from -154 to -67 per meg values ($\Delta'^{17}O_{rsw}$ of -67 to + 26 per meg)
477 and environments with AI values > 0.4 (semi-arid to humid environments) have $\Delta'^{17}O_{carb}$ carb
478 values that range from -86 to -60 per meg ($\Delta'^{17}O_{rsw}$ of -4 to + 27 per meg) (excluding one sample
479 collected from a depth of 7 cm, cp3, Table 2) (Figure 5). The mean $\Delta'^{17}O$ value of pedogenic
480 carbonates within each aridity class decreases with increasing aridity (Figure 5). The mean
481 $\Delta'^{17}O_{carb}$ values are -118 per meg (hyper-arid, n = 3), -92 per meg (arid, n = 13), -80 per meg
482 (semi-arid, n = 21), -77 per meg (dry sub-humid, n = 5), and -74 per meg (sub-humid, n = 1), and
483 -77 per meg (humid, n = 1) (Figure 5).

484 In soil carbonate samples from single profiles, we observed four profiles with $\delta^{18}O$ values
485 higher near the soil surface than at depth (20MOJrighthand, cp3 Tibet, GON07, CAN01). In
486 three of these four profiles, we measured low $\Delta'^{17}O_{rsw}$ values near the surface (Figure 6), and in
487 one of the profiles, we measured near-constant $\Delta'^{17}O_{rsw}$ values with depth. We documented two

profiles with near-constant $\delta^{18}O$ values with depth (NAC and Diablo); in those profiles we observed a decrease in $\Delta'^{17}O_{rsw}$ near the surface (NAC) and constant $\Delta'^{17}O_{rsw}$ (Diablo) (Figure 6).

We observed no covariation in $\delta^{18}O_{rsw}$ and $\Delta'^{17}O_{rsw}$ amongst the samples altogether (Figure 4), which is as expected given that the soils are forming from pore water with disparate initial $\delta^{18}O$ values and varying degrees of evaporation. We did observe covariation between 'normalized' $\delta^{18}O$ (calculated as $\delta^{18}O_{rsw}$ minus $\delta^{18}O_{ann}$) and $\Delta'^{17}O_{rsw}$ (Figure 4C). Covariation due to evaporation (or lack thereof) in $\delta^{18}O$ and $\Delta'^{17}O$ in related samples is described on a case basis as examples for paleoclimate applications (Section 4.5, Figure 7). We observed a wedge-like pattern between $\delta^{13}C$ and $\Delta'^{17}O_{carb}$ (Figure S13). This pattern might indicate increased soil water evaporation in mixed C_3-C_4 and in C_4-dominant ecosystems (grass and shrublands) compared to C_3-dominant ecosystems, or that respiration rates are especially low in some soils that experienced a lot of evaporation. It could also be related to an oversampling of C_4 ecosystems due to the large number of samples from the Serengeti (Beverly et al., 2021).

4. Discussion

4.1 Theoretical predictions for triple oxygen isotope patterns in soil waters

The predicted direction and magnitude of isotopic offset due to evaporation is instructive for natural soil carbonates, even though they are unlikely to have formed in the quasi-steady state conditions invoked for the Barnes and Allison (1983) model (i.e., upward diffusion of water from the water table, and no vapor transport below an evaporation front). The model predicts that evaporation of soil water should lead to the following patterns: (1) an increase in $\delta^{18}O$ and decrease in $\Delta'^{17}O$ relative to input water, with increasing fractionation within the top 0.1 to 0.3

m, (2) increased isotopic offset with decreasing relative humidity of the atmosphere, and (3) maximum evaporative offsets large enough to influence paleoclimate applications, if they are indeed recorded in pedogenic carbonates (Figure 2). Future work could compare these predictions by modifying other models of δ^2H and $\delta^{18}O$ in soil water, such as drying from a saturated soil (Zimmerman et al., 1967; Chamberlain et al., 2014) and time-varying models (Mathieu and Bariac, 1996; Zhou et al., 2021).

The apparent λ_{soil} values from the soil water evaporation model (median value of 0.517) are within the range of reported slopes resulting from progressive evaporation of a water body (i.e., λ_{lake}) (Barkan and Luz, 2007; Luz and Barkan, 2010; Surma et al., 2015, 2018; Gázquez et al., 2018; Passey and Ji, 2019; Voigt et al., 2021; Katz et al., 2023) (Figure S3). The median of the slopes of a linear model in $\delta^{18}O$-δ^2H space (2.5) is consistent with theoretical values for evaporation trajectories reported elsewhere based on the Craig-Gordon (1965) model (Barnes and Allison, 1988; Benettin et al., 2018; Bowen et al., 2018; Shi et al., 2021). However, in natural soil waters, the $\delta^{18}O$-δ^2H trajectories have slopes of 5-6 ‰ as a result of mixing between antecedent pore water and isotopically variant incoming precipitation (Gibson et al., 2008; Oerter and Bowen, 2017; Sprenger et al., 2017; Benettin et al., 2018). By extension, we expect that the $\delta'^{18}O$-$\delta'^{17}O$ relationships (λ_{soil}) in natural soil waters and carbonates would be steeper than the theoretically predicted values due to mixing. Our model-based predictions for λ_{soil} remain to be validated through studies of triple oxygen isotope compositions in natural soil pore waters.

4.2 Empirical evidence for prevalent evaporation in pedogenic carbonate parent waters

Our data suggest that non-negligible evaporation of parent soil waters is common across a variety of climate regimes (Figure 4). Evaporation is the most parsimonious explanation for the

observation that the $\Delta'^{17}O_{rsw}$ values from pedogenic carbonates tend to be lower (by up to ~60 per meg) than the $\Delta'^{17}O$ values of unevaporated global meteoric waters ($\Delta'^{17}O_{mw}$), which are typically 20-40 per meg (Aron et al., 2021a) (Figure 4). Evaporation in soil pore waters has been shown previously (Evaristo et al., 2015; Sprenger and Allen, 2020); our data add that these evaporated soil waters are commonly the host waters from which pedogenic carbonates form. While we favor evaporation as the dominant process responsible for lowering $\Delta'^{17}O$ in soil carbonates, we discuss the potential role of two other processes: isotopic disequilibrium and mixing.

We cannot strictly rule out the possibility that soil carbonate precipitated under periods of isotopic disequilibrium due to CO_2 degassing. Theoretical predictions suggest that CO_2 degassing would result in offsets in the $\delta^{18}O$ and $\Delta'^{17}O$ values of the dissolved inorganic carbon (DIC) species of up to +8 ‰ and +70 per meg, respectively, that could be inherited by the mineral (Guo and Zhou, 2019). The factors that drive calcite precipitation in soils (temperature, water content, and/or CO_2) generally change slowly (days to weeks) at the soil depths we sampled (e.g., Huth et al., 2019), much slower than DIC equilibration timescales (hours) (Uchikawa and Zeebe, 2012; Guo and Zhou, 2019), and the mineral remains buffered in the pore water (unlike stalagmites, for example). Furthermore, there is no evidence for widespread or large kinetic isotope effects: soil carbonate $\delta^{13}C$, $\delta^{18}O$ and Δ_{47} values generally conform with expectations (Cerling et al., 1989; Cerling and Quade, 1993; Quade et al., 2013) except in cryogenic environments (Burgener et al., 2018). We observe almost no $\Delta^{17}O_{rsw}$ values that are higher than the range of $\Delta^{17}O_{rsw}$ values. We suggest that kinetic isotope effects due to degassing are either small or nonexistent in the soils in this dataset. Equilibrium formation of soil carbonates could be tested more robustly with Δ_{47}-Δ_{48} clumped isotope thermometry (Fiebig et al., 2019; Guo, 2020).

Due to the nonlinearity in $\Delta'^{17}O$ notation, mixing between waters with different $\delta^{18}O$ values but the same $\Delta'^{17}O$ values results in a lower $\Delta'^{17}O$ value (e.g., Aron et al., 2021a). The signal due to nonlinearity is small compared to the observed offset between $\Delta'^{17}O_{rsw}$ and typical $\Delta'^{17}O_{mw}$ in our soil carbonate data. For example, as an estimate of the maximum lowering in $\Delta'^{17}O$ due to nonlinear mixing, we consider a mix of equal proportions of waters that differ in $\delta^{18}O$ by 20 ‰ with identical $\Delta'^{17}O$ values (i.e., two successive rainfall events with $\delta^{18}O$ values that spans the typical seasonal range at midlatitudes). This scenario results in a mixed water with a $\Delta'^{17}O$ value that is about 10 per meg lower than the starting value. Achieving a lowering in $\Delta'^{17}O$ that would completely explain the offset between $\Delta'^{17}O_{rsw}$ and typical $\Delta'^{17}O_{mw}$ (i.e., a lowering of ~60 per meg) through nonlinearity alone would require a 50% mix of two rain events that differ in $\delta^{18}O$ by >40 ‰. That scenario is unlikely to occur in natural settings. Thus, nonlinearity in mixing alone could contribute a minor amount (~10 per meg) but does not fully explain the observed low $\Delta'^{17}O_{rsw}$ values.

However, successive mixing between isotopically light rainfall and evaporatively enriched soil water is important to consider (e.g., Sprenger et al., 2016). The resulting mixed rain-soil water will have an isotopic composition that reflects some of the antecedent evaporation. A 50/50 mix between highly evaporated soil pore water ($\delta^{18}O$ = +20, $\Delta'^{17}O$ = -200 per meg) and isotopically light incoming precipitation ($\delta^{18}O$ = -20, $\Delta'^{17}O$ = +32) would result in soil water with an intermediate composition ($\delta^{18}O$ = 0 and $\Delta'^{17}O$ = -110). In a mix of the same endmembers but with a smaller fraction of antecedent, highly evaporated soil water (i.e., 10%), the resulting water will more closely resemble recharge (resulting in 'mixed' water with $\delta^{18}O$ = -16‰, $\Delta'^{17}O$ = -9 per meg). Thus, mixing with antecedent evaporated soil water is very likely to contribute to the observed low $\Delta'^{17}O_{rsw}$ values.

580 If evaporation is driving the lowering of $\Delta'^{17}O_{rsw}$ relative to typical global meteoric
581 waters, it should be accompanied by an increase in $\delta^{18}O_{rsw}$ values compared to the $\delta^{18}O$ of
582 recharge waters (Figure 1, Figure 2). In practice, this is difficult to definitively show because we
583 do not know the $\delta^{18}O$ values of recharge water; we used $\delta^{18}O_{ann}$ as a first approximation (Figure
584 4C) (Figure S15 shows the correlation using $\delta^{18}O$ of precipitation during the approximated
585 season of soil carbonate formation). $\delta^{18}O_{rsw}$ is often greater than $\delta^{18}O_{ann}$, a finding that is
586 consistent with evaporative modification of soil water and has been previously documented
587 (Quade et al., 2007a; Kelson et al., 2020; Beverly et al., 2021) (Figure 4B). Our pedogenic
588 carbonate data show that low $\Delta'^{17}O_{rsw}$ values generally co-occur with $\delta^{18}O_{rsw}$ values that exceed
589 $\delta^{18}O_{ann}$ (Figure 4C), providing strong evidence in favor of evaporation driving fractionation of
590 oxygen isotopes in soil water. Based on our data and typical evaporation slopes in triple oxygen
591 isotopes, we estimate that enrichments in $\delta^{18}O$ on the order of 1–5 ‰ are common
592 (corresponding to depletions in $\Delta'^{17}O$ of approximately 10 to 50 per meg). The apparently
593 commonplace signal of evaporation has significant implications for paleoclimate reconstructions
594 that center around interpretations of $\delta^{18}O_{carb}$.
595 One source of uncertainty is that we are inferring evaporation by comparing $\Delta'^{17}O_{rsw}$ to
596 $\Delta'^{17}O$ of meteoric waters (Figure 4). There is uncertainty in the calculated $\Delta'^{17}O_{rsw}$ values that is
597 introduced by uncertainty in the λ_{cc-w} value used to calculate water values from carbonates
598 (Bergel et al., 2020; Voarintsoa et al., 2020; Wostbrock et al., 2020a; Huth et al., 2022; Kelson et
599 al., 2022) (Section 2.4.3). Lower λ_{cc-w} values result in higher $\Delta'^{17}O_{rsw}$ values, which would
600 imply less evaporation overall in our dataset. One estimate of the error in λ_{cc-w} is ± 0.00021,
601 which is ± 1 S.D. of measured λ_{cc-w} values from 8 paired carbonate-water samples in our
602 laboratory (Huth et al., 2022; Kelson et al., 2022); this uncertainty translates to a maximum

603 difference in $\Delta'^{17}O_{rsw}$ of 13 per meg in the pedogenic carbonate samples. When $\Delta'^{17}O_{rsw}$ values
604 are calculated using the maximum λ_{cc-w} value, the $\Delta'^{17}O_{rsw}$ values remain distinct from global
605 meteoric waters, and the negative trend between $\delta'^{18}O_{rsw}$ and $\Delta'^{17}O_{rsw}$ remains (Figure S15).
606 Improved constraints on λ_{cc-w} in the future would allow us to revise the $\Delta'^{17}O_{rsw}$ values and to
607 precisely estimate the magnitude of evaporation in each of the reconstructed soil water values;
608 but it is unlikely to alter our main interpretation that many $\Delta'^{17}O_{rsw}$ values are evaporatively
609 modified.
610
611 *4.3 Depth profiles of $\Delta'^{17}O$ and $\delta^{18}O$ in natural soils*
612 We examine $\delta^{18}O$ and $\Delta'^{17}O$ values at multiple depths in natural soils to evaluate if $\Delta'^{17}O$
613 adheres to the expected depth-dependent patterns for evaporation. The soil profiles also allow us
614 to re-evaluate the assumption made in many paleoclimate applications that pedogenic carbonate
615 from depths > 40 cm records unevaporated soil water (Barnes and Allison, 1983; Allison et al.,
616 1983; Quade et al., 1989; Pendall et al., 1994; Liu et al., 1995, 1996; Oerter and Amundson,
617 2016; Kelson et al., 2020; Fischer-Femal and Bowen, 2021).
618 First, we examine if $\delta^{18}O$-$\Delta'^{17}O$-depth relationships in natural soils generally agree with
619 theoretical predictions that evaporation should result in higher $\delta^{18}O$ and lower $\Delta'^{17}O$ values in
620 shallower soil waters (0 to 40 cm) compared to deeper soil waters (Section 3.1, Figure 2) (for
621 $\delta^{18}O$ and $\delta^{2}H$: Barnes and Allison, 1983; Mathieu and Bariac, 1996; Hsieh et al., 1998; Zhou et
622 al., 2021). In four of the profiles, we observe higher $\delta^{18}O_{rsw}$ values coupled with lower $\Delta'^{17}O_{rsw}$
623 values at shallower depths (Figure 6; 20MOJrighthand, cp3, GON07, CAN01) (Figure S4
624 compares the Barnes and Allison 1983 model and the cp3 profile). Additionally, in each of these
625 four profiles, the shallow-sample $\delta^{18}O_{rsw}$ is high compared to the possible range of $\delta^{18}O$ of

626 precipitation and $\Delta'^{17}O_{rsw}$ is low compared to typical $\Delta'^{17}O_{mw}$ values. Evaporation likely drives
627 fractionation in these soil pore waters and is recorded in the pedogenic carbonates.
628 The inverse of this prediction is that if evaporation is unimportant, and no other processes
629 affect the oxygen isotope values of soil water (i.e., seasonal deep recharge), there should be no
630 variation in $\delta^{18}O$ or $\Delta'^{17}O$ with depth, and both values should reflect possible pristine $\delta^{18}O$ /$\Delta'^{17}O$
631 water values. In Diablo, a soil from the Coast Ranges of California, $\delta^{18}O$ and $\Delta'^{17}O$ values are
632 constant within the depths examined (50 and 80 cm). The $\delta^{18}O_{rsw}$ and $\Delta'^{17}O_{rsw}$ values are within
633 ranges expected for meteoric waters (Figure 6). This soil profile conforms with theoretical
634 predictions that evaporation should not affect the oxygen isotope values of soil water at depths
635 greater than 30 to 40 cm (shallower carbonate did not exist at this location) (Figure 6). This
636 sample has a relatively cold clumped isotope temperature that suggests carbonate formation
637 during the winter wet season. Additional study of the seasonal dynamics of pedogenic carbonate
638 formation and soil water recharge at this site would be needed to explain why pedogenic
639 carbonates form in un- or minorly- evaporated water (e.g., Gallagher and Sheldon, 2016; Huth et
640 al., 2019; Kelson et al., 2020).
641 We observed one soil profile that does not conform to predictions for either the absence
642 or presence of evaporation. In the NAC profile from the Ñacuñán Biosphere Reserve in the
643 Andean piedmont, Argentina (Ringham et al., 2016), $\delta^{18}O_{rsw}$ values are constant with depth and
644 resemble $\delta^{18}O_{ann}$, suggesting minor to no evaporation (Figure 6). In contrast, the $\Delta'^{17}O_{rsw}$ values
645 at both depths are lower than typical $\Delta'^{17}O_{mw}$ values, and the 50 cm sample has a value that is 17
646 per meg lower than the 100 cm sample, suggesting that evaporation could have played a role. We
647 hypothesize that the soil carbonate near the surface and at depths formed at different times of the

year as precipitation events from different seasons percolated to different depths, resulting in a complex isotopic profile (Peters et al., 2013; Ringham et al., 2016).

From this dataset, it is not clear which conditions allow for evaporation to be preserved in pedogenic carbonate depth profiles. The four sites with clear evidence for near-surface evaporation in their pedogenic carbonates represent disparate climates, latitudes, and elevations (Figure 6; 20MOJrighthand, cp3, GON07, CAN01) (Table 1). One similarity might be relatively coarse soil texture (presence of gravel) that enables evaporation. Surprisingly, the NAC and CAN01 sites yield different results with respect to apparent evaporation recorded in $\delta^{18}O_{rsw}$ and $\Delta'^{17}O_{rsw}$ but are only about ~200 km apart and formed under similar climates. Possible differences are increased plant productivity/density at NAC (Ringham et al., 2016) or carbonate morphology (the NAC sample is a from a profile developed in a sandy substrate with early stage carbonate nodule formation while CAN01 is a clast undercoating from a conglomeratic substrate). We hypothesize that various factors including soil texture, plant water redistribution, precipitation regime, and the timing of pedogenic carbonate formation relative to recharge events will converge to produce a simple, evaporation-driven profile vs. a more complex, or un-evaporated pedogenic profile (e.g., Cerling and Quade, 1993; Ringham et al., 2016; Kelson et al., 2020).

Next, we turn to the question of whether paleoclimate workers can rely on soil carbonates collected at depths > 40 cm to record unevaporated meteoric water values. A comparison between $\Delta'^{17}O_{rsw}$ and typical $\Delta'^{17}O_{mw}$ values of the pedogenic carbonates at depths > 50 cm suggest that evaporation has modified the isotopic composition of 'deep' soil water in all but one soil profile. In five of the six profiles, $\Delta'^{17}O_{rsw}$ is lower than typical $\Delta'^{17}O_{mw}$ values at all depths (Figure 6). It is plausible that differences between $\Delta'^{17}O_{rsw}$ and $\Delta'^{17}O_{mw}$ that are on the order of 20

per meg could be eliminated if local $\Delta'^{17}O_{mw}$ is much lower than typical values and/or if λ_{cc-w} is lower than we estimate, potentially reducing the apparent commonality of evaporated soil waters at depths below 40 cm. Even with this uncertainty, our soil profile data suggest that evaporation can be recorded in pedogenic carbonates from depths > 40 cm. Furthermore, evaporative modification might be difficult to detect with $\delta^{18}O$ alone because evaporation can modify soil waters at all depths, leaving little depth variation in $\delta^{18}O$ (NAC profile, Figure 6G). In this regard, our observations do not match the steady-state model predictions of minimal evaporation at depths typical of calcite horizon formation (i.e., minimal evaporation below 30 to 40 cm) (Barnes and Allison 1983) – highlighting that steady-state conditions are not representative of natural soils. Our observation is consistent with other evidence for evaporation in 'deep' soil pore waters (DePaolo et al., 2004). We hypothesize that shallower soil water and/or pre-evaporated surface water percolates to depths below 40 cm in these calcic soils, perhaps after mixing with newly infiltrated waters (Gazis and Feng, 2004; Sprenger et al., 2018). A better understanding of how evaporated soil water is transmitted to typical Bk horizon depths and recorded by carbonates could be achieved with a model of the isotopic composition of soil water that considers vapor flux, non-steady state (time-varying) conditions (Mathieu and Bariac, 1996; Zhou et al., 2021), and calcite solubility (Meyer et al., 2014; Huth et al., 2019; Domínguez-Villar et al., 2022).

4.4 A threshold relationship between aridity and $\Delta'^{17}O$ of pedogenic carbonates on a global scale

We expected to find a relationship between $\Delta'^{17}O$ of pedogenic carbonate and aridity, where aridity would promote soil water evaporation and lower $\Delta'^{17}O$ values of pedogenic carbonates (Amin et al., 2020; Beverly et al., 2021). We find a wedge-like relationship between

694 $\Delta'^{17}O$ and aridity on a global scale (Figure 5). Evaporation (low $\Delta'^{17}O_{carb}$ values) is more
695 common in arid environments, but pedogenic carbonates that formed from unevaporated pore
696 waters exist even in arid localities (Figure 5). Humid environments are poorly represented in the
697 dataset (in part because soil carbonates are less common in humid compared with drier
698 environments), but the existing samples show uniformly high $\Delta'^{17}O_{carb}$ values that indicate little
699 to no soil water evaporation. We hypothesize that the variation in $\Delta'^{17}O$ in each aridity class on a
700 global basis is due to differences in input $\Delta'^{17}O$ of local meteoric waters, effects relating to
701 vegetation, the age of the pedogenic carbonates, and the dynamics of pedogenic carbonate
702 formation, as described below.
703 Differences in the input $\Delta'^{17}O_{mw}$ may complicate the relationship between $\Delta'^{17}O_{carb}$ and
704 aridity on a global scale (Figure 5, Figure S14). $\Delta'^{17}O_{mw}$ sets the local starting value from which
705 soil waters will isotopically evolve during evaporation (Figure 1). $\Delta'^{17}O_{mw}$ of global meteoric
706 waters are relatively invariant, with a mean of 33 per meg and 1 SD of 12 per meg (n = 1557,
707 Aron et al., 2021). If we use global meteoric water to guide site-specific estimates of $\Delta'^{17}O_{mw}$, we
708 find that the difference between $\Delta'^{17}O_{rsw}$ and $\Delta'^{17}O_{mw}$ at the sites has a strong relationship with
709 aridity (Figure S14) (largely because mean $\Delta'^{17}O_{mw}$ is relatively invariant). However, we caution
710 that $\Delta'^{17}O_{mw}$ values based on averages could diverge significantly from the true $\Delta'^{17}O_{mw}$ values.
711 First, $\Delta'^{17}O_{mw}$ can vary with season (Aron et al., 2023). Second, though atypical, there are
712 examples of rain and tap water with $\Delta'^{17}O$ values < 0 per meg due to raindrop re-evaporation in
713 the sub-cloud (Landais et al., 2010; Risi et al., 2013; Li et al., 2015; Giménez et al., 2021; Aron
714 et al., 2023; Xia et al., 2023). It is possible that input water with very low (<0 per meg) $\Delta'^{17}O$
715 values could partially contribute to lowering the observed $\Delta'^{17}O_{rsw}$ values, especially in arid
716 environments, though the extent to which these very low (<0 per meg) $\Delta'^{17}O$ precipitation events

717 contribute significantly to recharging soil water is unknown. Future work that characterizes input
718 $\Delta'^{17}O_{mw}$ is needed to be able to understand $\Delta'^{17}O_{rsw}$ and its relationship with aridity.
719 Vegetation (or lack thereof) may play a role in the observed pattern between $\Delta'^{17}O_{rsw}$ and
720 aridity. First, the sparseness of the vegetation at the more arid sites could contribute to higher
721 surface temperatures and increased evaporation from soils. Second, because transpiration does
722 not alter the isotopic composition of soil water (Ehleringer and Dawson, 1992) but evaporation
723 does, an increased ratio of transpiration to evaporation in the soil dewatering that precedes soil
724 carbonate formation could contribute to the higher $\Delta'^{17}O_{rsw}$ values observed in more humid (more
725 vegetated) environments (Barnes and Allison 1983). Furthermore, plants can redistribute water
726 in the soil profile, as documented through measurements of oxygen and hydrogen isotope ratios,
727 altering the vertical profiles of the isotopic composition of water and the soil moisture content
728 (Caldwell et al., 1998; Oerter and Bowen, 2019). Differing vegetation (e.g., desert shrubs vs.
729 grasses vs. trees) and their water sourcing strategies could account for some of the variation in
730 $\Delta'^{17}O_{rsw}$ amongst aridity classes. In this dataset, grasslands and shrublands are overrepresented;
731 future workers may wish to investigate $\Delta'^{17}O_{carb}$ in forested environments where we might expect
732 less evaporation (Railsback, 2021).
733 One limitation of the current dataset is that some of the sites have poor constraints on the
734 age and duration of pedogenic carbonate formation (Supplementary Text Section 2). It is
735 possible that some of the variation in $\Delta'^{17}O_{rsw}$ within aridity classes is because some of the
736 pedogenic carbonates formed during climate conditions that were different than modern. For
737 example, the CA08-005-1 sample is from the north flank of the San Bernardino Mountains
738 (which delineate the Mojave Desert) and is late Pleistocene to middle Holocene in age (Passey et
739 al., 2010 and references within). In contrast, the MOJ-righthand samples from the Mojave Desert

740 of California are middle Holocene in age based on geomorphic context (Supplementary
741 Material). These sites are both in the Mojave Desert but yield differing $\Delta'^{17}O_{rsw}$ values, with the
742 MOJ-righthand samples being significantly lower (Table 2). Differences in age might be a factor,
743 especially given that the late Pleistocene was wetter than the Holocene in the Mojave Desert
744 (McDonald et al., 2003). Other factors include geomorphic surface (breccia landslide vs. coarse
745 alluvial fan) or true differences in aridity (CA08-005-1 is at the edge of the Mojave Desert while
746 MOJ-righthand is well within the Mojave Desert).

747 We hypothesize that the dynamics of pedogenic carbonate formation contributes to the
748 wedge-like relationship between $\Delta'^{17}O_{carb}$ and aridity through factors including depth, timing,
749 and variation in the processes driving crystallization. Variation in the relative depths of
750 pedogenic carbonate formation and the evaporation front could contribute to some of the
751 variability in $\Delta'^{17}O_{carb}$ (and $\Delta'^{17}O_{rsw}$) within aridity classes. The depth to which evaporative
752 isotopic fractionation propagates into the soil depends on environmental factors including
753 evaporation rates, relative humidity of the atmosphere, and physical soil characteristics (Figure
754 S1). The depth of carbonate formation is also related to climate and soil texture (Retallack,
755 2005). How these factors combine to create conditions in which pedogenic carbonate forms
756 within versus below the evaporation front may be explored in the future with non-steady state
757 models of soil water and its isotopic composition, models of pedogenic carbonate formation, and
758 careful sampling of pedogenic carbonate from stable land surfaces.

759 The timing and processes driving pedogenic carbonate precipitation will control the
760 isotopic composition of the soil water that is recorded, including $\Delta'^{17}O_{rsw}$. There could be
761 discrepancies between annual average aridity conditions (i.e., AI) and the actual conditions
762 preceding and during pedogenic carbonate formation (Supplementary Text Section 3, Figures

763 S16, S17, S18) for discussion of seasonal estimates of AI). As a hypothetical example: in an arid
764 environment, pedogenic carbonate could form shortly following rain or infiltration events that
765 reset the isotopic composition of soil water (Snell et al., 2013; Huth et al., 2019). Thus, even if
766 soil water is highly evaporated on average, pedogenic carbonate may form during the initial
767 phases of evaporation, resulting in values of $\Delta'^{17}O_{rsw}$ and $\delta^{18}O_{rsw}$ that closely resemble input
768 precipitation. This mechanism could explain why we observe more variation in $\Delta'^{17}O$ values in
769 arid and semi-arid environments than in sub-humid and humid environments (although this could
770 also be due to under-sampling in humid environments). This hypothesis would predict that
771 rainfall intermittency and the seasonality of rainfall will be important in determining if
772 pedogenic carbonate records evaporative conditions (Peters et al., 2013; Tabor et al., 2013;
773 Gallagher and Sheldon, 2016; Huth et al., 2019).

774 Furthermore, there could be differing modes of pedogenic carbonate formation that relate
775 to aridity and contribute to the wedge-like relationship with $\Delta'^{17}O_{rsw}$. Pedogenic carbonate
776 formation can be driven by soil dewatering via evaporation or transpiration (e.g., Breecker et al.,
777 2009; Gallagher and Sheldon, 2016) or by fluctuations in biologically respired CO_2 (Mintz et al.,
778 2011; Zamanian et al., 2016). We expect that in more arid environments, evaporation-driven
779 dewatering may drive pedogenic carbonate precipitation, resulting in lower $\Delta'^{17}O_{rsw}$ values. In
780 more humid environments, fluctuations in soil CO_2 and/or plant dewatering may drive pedogenic
781 carbonate precipitation, resulting in higher $\Delta'^{17}O_{rsw}$ values. This idea remains to be
782 systematically tested.

783 The pedogenic carbonate from the Atacama Desert (Quade et al., 2007b) illustrates that
784 relatively minimal evaporation can be recorded by pedogenic carbonates in arid environments.
785 The Atacama Desert is one of the driest places in the world, with a mean annual precipitation of

< 100 mm/year and sparse vegetation. If the degree of soil water evaporation at the time of pedogenic carbonate formation were solely based on aridity, we would expect the $\Delta'^{17}O_{rsw}$ value of this sample to be among the lowest observed. However, we measure a $\Delta'^{17}O$ value that is near the median of the $\Delta'^{17}O$ of globally observed values (median $\Delta'^{17}O_{rsw}$ = 3 per meg, Atacama $\Delta'^{17}O_{rsw}$ = 9 per meg). In theory, high input $\Delta'^{17}O_{mw}$ could mask a high magnitude of evaporation in soil waters (low $\Delta'^{17}O_{rsw}$). One study shows that in the Andes, $\Delta'^{17}O$ values of precipitation can be as high as 40 to 50 per meg, although most are within the more typical range of 20 to 40 per meg (Aron et al., 2021b). Surma et al. (2018) report groundwater and tap water with $\Delta'^{17}O$ values of +7 and + 11 per meg from the Salar de Llamara, a lower-elevation salt flat in the Atacama Desert. Local constraints on input $\Delta'^{17}O_{mw}$ is required to fully evaluate if high input $\Delta'^{17}O_{mw}$ is responsible for the relatively high $\Delta'^{17}O_{rsw}$ at the Atacama Desert and elsewhere. Another possible explanation is that the soil water evaporation front (z_{ef}) is above the pedogenic carbonate formation (115 cm). In the steady-state model of the isotopic composition of soil water (Section 2.1, Barnes and Allison [1983]), a high evaporation rate results in a large but shallow evaporative signal as unevaporated liquid water is advected upward and counteracts diffusion of evaporated soil water (Figure S1). Another hypothesis is that in this extremely arid environment, pedogenic carbonate forms soon after infiltration events, resulting in pedogenic carbonates that appear only moderately evaporated as rainwater overwhelms the isotopic composition of residual evaporated water. This could be true even if soil water is highly evaporated during most of the year. The climatologic, hydrologic, and soil factors that contribute to the evaporative state of soil water at the depth and time of soil carbonate formation is a topic for future study at well-constrained localities.

4.5 Examples for paleoclimate applications: $\Delta'^{17}O$ reveals drivers of $\delta^{18}O$ variation in geographically related samples

In this section, we describe how $\Delta'^{17}O_{carb}$ can be used to investigate the causes of variation in $\delta^{18}O$ and can help reconstruct evaporation, precipitation sources, soil hydrologic processes, and elevations in ancient systems. We draw from examples of geographically related pedogenic carbonates in this dataset.

First, we demonstrate how to identify evaporation and improve estimates of un-evaporated $\delta^{18}O$ of meteoric waters using a suite of samples and their $\delta^{18}O$-$\Delta'^{17}O$ covariation across a landscape. As first reported in Beverly et al. (2021), pedogenic carbonates sampled across an aridity gradient in Serengeti, Tanzania, record varying amounts of evaporation in soil water (Figure 7A). The most arid sites have the lowest $\Delta'^{17}O$ values and the highest $\delta^{18}O$ values. A linear trend between $\delta^{18}O$ and $\Delta'^{17}O$ of the Serengeti samples yields a change of -7.4 per meg/‰ (r^2 = 0.78), corresponding to a $\delta'^{18}O$-$\delta'^{17}O$ slope (λ_{soil}) of 0.5206. This slope is within the range of triple oxygen isotope evaporation slopes predicted in the steady state soils model (Section 3.1). Thus, evaporation can explain the variation in $\delta^{18}O$ at this location. By extension, we hypothesize that the pedogenic carbonates formed in soil waters with a similar starting $\delta^{18}O$ value that experienced varying degrees of evaporation. The linear regression of $\delta'^{18}O$-$\Delta'^{17}O$ points back to a recharge $\delta^{18}O$ of about -2 to -3 ‰ assuming a $\Delta'^{17}O_{mw}$ of 30 to 40 per meg (Figure 7A). This approximate recharge $\delta^{18}O$ value is similar to the reported $\delta^{18}O$ values from local spring and river water (Beverly et al., 2021). The accuracy of this kind of reconstruction of the recharge water $\delta^{18}O$ is subject to uncertainties in $\Delta'^{17}O_{mw}$ and even in the existence of a single source water $\delta^{18}O$ (Benettin et al., 2018). However, the Serengeti samples hint that such an approach might be possible and could be developed with improved theoretical and empirical

constraints on $\delta'^{18}O$-$\Delta'^{17}O$ slopes across climate regimes (analogous to the Passey and Ji [2019] approach for lakes). Even with the stated uncertainties, the $\Delta'^{17}O$-informed estimate of the $\delta^{18}O$ of source water made is much closer to the true value than the 'face value' estimate from $\delta^{18}O_{carb}$. Future workers could employ suites of samples and $\delta^{18}O$-$\Delta'^{17}O$ covariation to identify evaporation in the geologic record.

We show that $\Delta'^{17}O$ can identify differences in the $\delta^{18}O$ values of moisture sources, in part by ruling out evaporation. We documented one region where $\Delta'^{17}O$ shows that variation in $\delta^{18}O$ is not driven by evaporation: pedogenic carbonates from monsoonal, tropical Myanmar (Figure 7B). Pedogenic carbonates were sampled across a rainfall gradient in central "dry" belt of Myanmar, which is in the rain shadow of the Indo-Burman Ranges and has precipitation of <1000 mm/year. The pedogenic carbonates display a range in $\delta^{18}O_{carb}$ of -8.6 to -1.5 ‰, all collected from depths > 50 cm. In these samples, lower $\delta^{18}O$ values occur at the driest localities, leading previous workers to hypothesize that the variation in $\delta^{18}O$ was due to variation in the seasonal timing of carbonate formation and seasonal variation in parent soil water $\delta^{18}O$ (Licht et al., 2022). We measured $\Delta'^{17}O$ of the carbonates from the driest and wettest locality based on MAP (1100 mm/year and 760 mm/year for 19ND04 and 20ND03 respectively, $\delta^{18}O_{rsw}$ of -1.3 and -5.8 ‰). We observe no variation in $\Delta'^{17}O$ in the two measured samples within our precision ($\Delta'^{17}O_{rsw}$ of +6 and +4 per meg). The lack of variation in $\Delta'^{17}O_{rsw}$ in the two samples supports the idea that $\delta^{18}O$ variation is not due to evaporation. Instead, $\delta^{18}O$ variation in this setting could be due to a difference in the timing of pedogenic carbonate formation and seasonal variation in recharge water $\delta^{18}O$, which should be driven by distillation-type processes and result in no variation in $\Delta'^{17}O_{rsw}$ in resulting carbonate.

In some soils, $\Delta'^{17}O$ values can be used to test hypotheses about hydrologic processes, like soil water mixing with depth. Amongst the samples from Vertisols in a chronosequence of terraces along the Brazos River in Texas, we observed uniformity in $\delta^{18}O$ and $\Delta'^{17}O$ (Figure 7C). Vertisols are defined by their high clay content and vertical cracks that propagate from the surface downward (Nordt et al., 2004; Kovda, 2020). The large cracks might suggest a high proportion of evaporative soil-dewatering given the large porosity and small tortuosity allowing for rapid vapor transport, which would result in low $\Delta'^{17}O_{sw}$ values and high $\delta^{18}O_{sw}$ values, but they may also lead to rapid down-profile transit of meteoric waters with minimal evaporation (Kovda et al., 2006; Kovda, 2020). The $\Delta'^{17}O_{rsw}$ values of the group of soils from Texas suggests only minor evaporation compared to meteoric waters ($\Delta'^{17}O_{rsw}$ of -2 to + 10 per meg), in line with other studies of Vertisols from Texas that have invariant $\delta^{18}O$ values that are similar to meteoric water $\delta^{18}O$ (Kovda et al., 2006; Miller et al., 2007). In this group of samples, the lack of variation in $\Delta'^{17}O_{rsw}$ and $\delta^{18}O_{rsw}$ suggests that moderately evaporated soil waters are well-mixed in a Vertisol or that pedogenic carbonate is physically mixed during pedoturbation. $\Delta'^{17}O_{rsw}$ lends credibility to the interpretation that $\delta^{18}O_{rsw}$ values are only slightly evaporated and provides insights into soil water hydrology in Vertisols.

The soil carbonate samples from the Iranian plateau demonstrate that $\Delta'^{17}O_{rsw}$ can be used to better understand $\delta^{18}O$-elevation relationships but that complexities persist in using $\delta^{18}O$ values for paleoaltimetry. $\delta^{18}O$-based paleoaltimetry uses the depletion of ^{18}O during rain-out of uplifting air masses, as recorded in authigenic minerals, to reconstruct past elevations (Poage and Chamberlain, 2001; Rowley, 2007; Mulch, 2016). However, in arid plateaus this framework is invalidated if rainfall is recycled or if moisture source varies regionally, resulting in $\delta^{18}O$ that remains constant or even increases with elevation up and across a plateau (Bershaw et al., 2012;

877 Li and Garzione, 2017; Cassel et al., 2018; Caves Rugenstein and Chamberlain, 2018; Aron et
878 al., 2021b). Indeed, we observe that the soil carbonates from the Iranian plateau that are
879 separated by 1.5 km in elevation have $\delta^{18}O_{rsw}$ values within 1 ‰ of each other (Figure 7D), a
880 lapse rate that is far lower than a typical 3‰/km driven by uplift and distillation of air masses
881 (Rowley, 2007). The soil carbonate samples have $\Delta'^{17}O_{rsw}$ that are the same within current
882 precision and are moderately evaporated compared to typical $\Delta'^{17}O_{mw}$ values (Figure 7D). The
883 similarity in $\delta^{18}O_{rsw}$ and $\Delta'^{17}O_{rsw}$ indicate that the isotopic composition of the higher elevation
884 sample could be a result from recycling of the same moisture source as the lower elevation
885 sample, which would lead to a slight increase in $\Delta'^{17}O$ and $\delta^{18}O$ (Bershaw et al., 2012; Surma et
886 al., 2021; Xia et al., 2023). It is also possible that the soil carbonates formed from distinct
887 moisture sources with similar isotopic compositions and similar degree of evaporation, given that
888 both the Caspian Sea and Mediterranean Sea source rainfall in this topographically complex
889 region (Evans et al., 2004). Information on the isotopic composition of various air masses and
890 trajectories is needed to fully understand the $\delta^{18}O$-elevation relationships in the soil carbonates of
891 the Iranian plateau. We remain optimistic that $\Delta'^{17}O_{rsw}$ could be used to identify moisture
892 recycling in the interior of high plateaus and thus better constrain paleo-elevation estimates.
893
894 *4.6 Implications for pedogenic carbonates in paleoclimate studies and recommendations for the*
895 *use and development of $\Delta'^{17}O$ in future studies*
896 Foremost, our data demonstrate that pedogenic carbonate in arid environments is likely to
897 form from water that is evaporatively enriched in ^{18}O by about 1–5 ‰, even at depths > 40 cm in
898 the soil profile. This finding may seem unsettling for terrestrial paleoclimate research that centers
899 around using pedogenic carbonate as a faithful record of meteoric water $\delta^{18}O$. For example,

ignoring evaporation could result in a misattribution of the moisture source of a region. One could underestimate the elevation of ancient mountains by 0.5–2 km, assuming a typical lapse rate of about 0.3 ‰/km (Poage and Chamberlain, 2001). Fortunately, $\Delta'^{17}O$ can be used to identify evaporation, and workers can leverage that information to improve estimates of pristine $\delta^{18}O$ and/or to infer environmental conditions and carbonate formation processes. Workers may not have to exhaustively analyze all samples in a $\delta^{18}O$-based paleoclimate record for $\Delta'^{17}O$, which is not feasible given that measuring $\Delta'^{17}O$ of carbonate is resource-intensive at the time of writing. Instead, workers may use $\delta^{18}O$ variations to target a subset of samples for $\Delta'^{17}O$ analysis. Choosing the samples that represent the observed minimum and maximum $\delta^{18}O$ values will most likely maximize the possible range in $\Delta'^{17}O$ and will allow workers to answer specific questions about the factors that drive variation in $\delta^{18}O$.

Future studies could use $\Delta'^{17}O$ to improve estimates of meteoric water $\delta^{18}O$ reconstructed from pedogenic carbonate. First, $\Delta'^{17}O_{rsw}$ can be compared to typical or site-specific $\Delta'^{17}O_{mw}$ values to determine if evaporation is likely. If $\Delta'^{17}O_{rsw}$ is well within range of $\Delta'^{17}O_{mw}$, one could deem evaporation unlikely and confidently interpret $\delta^{18}O_{rsw}$ as indicative of $\delta^{18}O_{mw}$. If evaporation has occurred, $\Delta'^{17}O_{rsw}$ - $\delta^{18}O_{rsw}$ trajectories could be used to reconstruct the $\delta^{18}O$ of the source waters and to estimate the magnitude of evaporation, similar to approaches in lakes (Passey and Ji, 2019; Katz et al., 2023), the example from the Serengeti soils in this paper, and source water determinations from $\delta^{18}O$ and $\delta^{2}H$ (Bowen et al., 2018). This type of reconstruction of unevaporated soil water $\delta^{18}O$ would require an estimate of unevaporated $\Delta'^{17}O_{mw}$, which sets the intersection with the meteoric water line, and could be determined via "unevaporated" sedimentary carbonates (i.e., flow-through lake carbonates, tufas, or speleothems, which may record similar $\Delta'^{17}O_{mw}$ but distinct $\delta^{18}O_{mw}$ from soils due to differences in proxy biases), or via

923 modern rainfall. Reconstructing unevaporated $\delta^{18}O$ and the magnitude of evaporation would also
924 require a determination of the slope of the evaporation line from either a suite of samples that
925 represent increasing evaporation (similar to the Serengeti samples of Beverly et al., 2021) and/or
926 from theory, analogous to slopes in $\delta^{18}O$-$\delta^{2}H$ space (Benettin et al., 2018; Bowen et al., 2018).

927 Workers could use $\Delta'^{17}O_{carb}$ to place broad constraints on aridity for past climates if the
928 present pattern of low $\Delta'^{17}O_{carb}$ values being common in semi-arid, arid, and hyper arid
929 environments and uncommon in sub-humid and humid climates holds up with additional
930 sampling. For example, if low $\Delta'^{17}O_{carb}$ values are observed ($\Delta'^{17}O_{carb} < -110$ per meg), there
931 would be high confidence that climates were semi-arid to hyper-arid. However, the observation
932 of high $\Delta'^{17}O_{carb}$ values would place less of a constraint on aridity, because these appear to be
933 possible across the full range of aridity. Workers who wish to use $\Delta'^{17}O_{carb}$ to track ancient
934 aridity in a more quantitative fashion might be able to do so on a regional basis by studying its
935 pattern in modern analog environments as in Beverly et al. (2021).

936 As we learn more about $\Delta'^{17}O_{carb}$, we may discover links between it and $\delta^{13}C$. The
937 dominant control on $\delta^{13}C$ of pedogenic carbonate is the photosynthetic pathway of overlying
938 vegetation (i.e., C_3 vs C_4) (Cerling and Quade, 1993). The type of vegetation (recorded by $\delta^{13}C$)
939 may have indirect effects on $\delta^{18}O$ and $\Delta'^{17}O$ of soil water via plant water use and/or shading.
940 Within a certain vegetation class, the availability of water can influence the $\delta^{13}C_{carb}$ and might be
941 reflected in $\Delta'^{17}O_{carb}$. For example, we might expect to find higher $\delta^{13}C$ and lower $\Delta'^{17}O_{carb}$
942 values during dry periods where microbial respiration is reduced (Conant et al., 2004), which
943 could lead to an decreased component of respired CO_2 in the soil (Cerling, 1984). In contrast,
944 low $\delta^{13}C$ and high $\Delta'^{17}O$ values might be associated with higher soil respiration rates, as soil
945 carbonate may be formed via biotic-driven fluctuations in CO_2 rates rather than soil drying. If

946 this relationship between $\Delta'^{17}O_{carb}$ and soil respiration rates proves to be robust, it could greatly
947 improve $\delta^{13}C$-based reconstructions of ancient atmospheric concentrations CO_2 that require an
948 assumption of soil respiration rate during pedogenic carbonate formation (Cerling, 1984), as
949 ancient soil respiration rates can be difficult to constrain (Breecker et al., 2010; Cotton and
950 Sheldon, 2012; Montañez, 2013; Fischer-Femal and Bowen, 2021).

951 Soil carbonates are a rich but complex archive, and we need to leverage every isotope
952 system we have to decipher environmental signals. Ultimately, the utility of $\Delta'^{17}O$ may be to
953 yield insights into soil carbonate formation processes and to will help build a proxy system
954 model for soil carbonates (Evans et al., 2013; Dee et al., 2016; Bowen et al., 2020; Fischer-
955 Femal and Bowen, 2021). To this end, future studies of $\Delta'^{17}O$ at well-studied modern soil
956 localities may seek to understand the environmental conditions that promote the presence of
957 evaporatively dominated soil waters during pedogenic carbonate formation. Integrating water
958 content data with data on the isotopic composition of meteoric and soil waters will allow workers
959 to separate the effects of mixing, transpiration, and evaporation to understand the source of soil
960 water. For example, the two Fish Lake Valley (FLV), Nevada, sites have distinct seasonal
961 patterns in soil water content that help explain the $\Delta'^{17}O_{rsw}$ and $\delta^{18}O_{rsw}$ (Oerter and Amundson,
962 2016). Site B has high variability in water content at depths < 40 cm, likely reflecting
963 evapotranspiration fluxes, possibly allowing for recharge and mixing of various generations of
964 water at shallower depths that are transmitted to greater depths. At this site, $\delta^{18}O_{rsw}$ (-8 ‰)
965 resembles summer rain, but might also represent a mix summer recharge and antecedent pore
966 water based on the relatively low $\Delta'^{17}O_{rsw}$ (-14 per meg) (Table 2). In comparison, site C had a
967 more consistent water content with a minimum at a depth of 50 cm that was attributed to plant
968 uptake (Oerter and Amundson, 2016). Site C had a $\delta^{18}O_{rsw}$ value that resembles winter rain (-13

969 ‰) and a slightly less evaporated $\Delta'^{17}O_{rsw}$ value (-7 per meg) (Table 2). At site C, the soil water
970 at depth might reflect winter storm events that percolate to at least 80 cm that were not observed
971 during the monitoring period. Process-based studies are key to understanding how and when soil
972 carbonate forms, the evaporation trajectory of parent waters, and the ultimate source of soil water
973 from which pedogenic carbonates form.
974
975 **5. Conclusions**
976 $\Delta'^{17}O_{carb}$ records the evaporative state of the soil water at the time of pedogenic carbonate
977 formation. We find that evaporative modification of $\Delta'^{17}O_{rsw}$ values is commonly recorded by
978 pedogenic carbonates, implying that evaporation is a concern for $\delta^{18}O_{carb}$-based paleoclimate
979 interpretations, especially from arid and/or sparsely vegetated settings. Paleoclimate workers
980 may use $\Delta'^{17}O$ to test for evaporation where a robust reconstruction of meteoric water $\delta^{18}O$ is
981 required (i.e., to reconstruct moisture recycling, paleo-elevations, air mass interactions, and
982 isotope gradients). This will enable more quantitative comparisons with isotope-enabled climate
983 models (Poage and Chamberlain, 2001; Winnick et al., 2014; van Dijk et al., 2020; Zhu et al.,
984 2020). While $\Delta'^{17}O_{carb}$ values are generally lower and more variable in more arid environments,
985 similar to the 'wedge' observed in mammal teeth (Lehmann et al., 2022), $\Delta'^{17}O_{carb}$ falls short as a
986 simple indicator of aridity across geographic regions. We suggest that $\Delta'^{17}O_{carb}$ will be most
987 useful in identifying when variation in $\delta^{18}O_{carb}$ is due to increased evaporation (i.e., in the
988 modern Serengeti samples) versus when variation in $\delta^{18}O_{carb}$ is due to a difference in recharge
989 $\delta^{18}O$ (i.e., in the modern Myanmar samples). In theory, a suite of a related samples with
990 evaporatively driven covariation in $\delta^{18}O$ and $\Delta'^{17}O$ could be used to reconstruct unevaporated
991 $\delta^{18}O$, although this approach remains to be validated in natural soil pore waters and carbonates.

This work reveals an incomplete understanding of the environmental factors, in addition to aridity, that control the evaporative state of soil water that is ultimately recorded by pedogenic carbonates. There remains uncertainty in how an evaporation signal is propagated downward in the soil profile, how the depth of the evaporation relates to the depth of calcic horizons in soils, and how the timing of evaporation relates to the timing of carbonate precipitation. $\Delta'^{17}O$ is poised to aid workers in studies of well-constrained localities to better understand the circumstances of pedogenic carbonate formation, which will ultimately improve our ability to understand the paleoclimate information that is recorded in their stable isotopes.

Acknowledgements

This research was supported by funding from U.S. National Science Foundation grant EAR-PF 1854873 to J.R. Kelson, EAR-PF 1725621 to E.J. Beverly, and EAR 2122023 to N. E. Levin. Collection of samples by A.M. Hudson was funded by the U.S. Geological Survey Mendenhall Postdoctoral Fellowship program. Work at LLNL was conducted under the auspices of DOE Contract DE-AC52-07NA27344, release number LLNL-JRNL-849216. We thank Drake Yarian, Sarah Katz, Natalie Packard, and Kirsten Andrews for assistance for triple oxygen isotope measurements and Ashling Neary, Elise Pelletier, and Kirsten Andrews, for assistance with clumped isotope measurements. This manuscript was improved based on comments from Weifu Guo, Julia McIntosh, and three anonymous reviewers. Any use of trade, firm, or product names is for descriptive purposes only and does not imply endorsement by the U.S. Government.

Appendix A: Supplementary Material

1014 The supplementary material to this article includes text, figures, and tables that give additional
1015 details regarding the Barnes and Allison (1983) soil physics model, the soil sites, and the
1016 methods for estimating the AI and $\delta^{18}O$ of precipitation during soil carbonate formation season.
1017 The supplementary material can be found online at (doi provided by GCA).
1018

1019 **Research Data**

1020 Research Data associated with this article, including individual measurements of triple oxygen
1021 and clumped isotope measurements of samples and standard materials, is accessible via
1022 EarthChem (https://doi.org/10.26022/IEDA/112737).
1023

References

Alexandre A., Landais A., Vallet-Coulomb C., Piel C., Devidal S., Pauchet S., Sonzogni C., Couapel M., Pasturel M., Cornuault P., Xin J., Mazur J. C., Prié F., Bentaleb I., Webb E., Chalié F. and Roy J. (2018) The triple oxygen isotope composition of phytoliths as a proxy of continental atmospheric humidity: Insights from climate chamber and climate transect calibrations. *Biogeosciences* **15**, 3223–3241.

Allison G. B., Barnes C. J. and Hughes M. W. (1983) The distribution of deuterium and ^{18}O in dry soils 2. Experimental. *J.Hydrol.* **64**, 377–397.

Amin A., Zuecco G., Geris J., Schwendenmann L., McDonnell J. J., Borga M. and Penna D. (2020) Depth distribution of soil water sourced by plants at the global scale: A new direct inference approach. *Ecohydrology* **13**, e2177.

Amundson R. G., Chadwick O. A., Sowers J. M. and Doner H. E. (1989) The Stable Isotope Chemistry of Pedogenic Carbonates at Kyle Canyon, Nevada. *Soil Sci. Soc. Am. J.* **53**, 201–210.

Amundson R. G., Franco-Vizcaino E., Graham R. C. and Deniro M. (1994) The Relationship of Precipitation Seasonality To the Flora and Stable-Isotope Chemistry of Soils in the Vizcaino Desert, Baja-California, Mexico. *J. Arid Environ.* **28**, 265–279.

Amundson R. G. and Lund L. J. (1987) The Stable Isotope Chemistry of a Native and Irrigated Typic Natrargid in the San Joaquin Valley of California1. *Soil Sci. Soc. Am. J.* **51**, 761–767.

Anderson N. T., Kelson J. R., Kele S., Daëron M., Bonifacie M., Horita J., Mackey T. J., John C. M., Kluge T., Petschnig P., Jost A. B., Huntington K. W., Bernasconi S. M. and Bergmann K. D. (2021) A Unified Clumped Isotope Thermometer Calibration (0.5–1,100°C) Using Carbonate-Based Standardization. *Geophys. Res. Lett.* **48**, 1–11.

Aron P. G., Levin N. E., Beverly E. J., Huth T. E., Passey B. H., Pelletier E. M., Poulsen C. J., Winkelstern I. Z. and Yarian D. A. (2021a) Triple oxygen isotopes in the water cycle. *Chem. Geol.*, 120026.

Aron P. G., Poulsen C. J., Fiorella R. P., Levin N. E., Acosta R. P., Yanites B. J. and Cassel E. J. (2021b) Variability and Controls on $\delta^{18}O$, d-excess, and $\Delta'^{17}O$ in Southern Peruvian Precipitation. *J. Geophys. Res. Atmos.* **126**, e2020JD034009.

Aron P. G., Li S., Brooks J. R., Welker J. M. and Levin N. E. (2023) Seasonal Variations in Triple Oxygen Isotope Ratios of Precipitation in the Western and Central United States. *Paleoceanogr. Paleoclimatol.* **38**, e2022PA004458.

Barkan E. and Luz B. (2007) Diffusivity fractionations of $H_2{}^{16}O/H_2{}^{17}O$ and $H_2{}^{16}O/H_2{}^{18}O$ in air and their implications for isotope hydrology. *Rapid Comm. Mass Spectrom.* **21**, 2999–3005.

Barkan E. and Luz B. (2005) High precision measurements of $^{17}O/^{16}O$ and $^{18}O/^{16}O$ ratios in H2O. *Rapid Comm. Mass Spectrom.* **19**, 3737–3742.

Barkan E., Musan I. and Luz B. (2015) High-precision measurements of $\delta^{17}O$ and ^{17}Oexcess of NBS19 and NBS18. *Rapid Comm. Mass Spectrom.* **29**, 2219–2224.

Barnes C. J. and Allison G. B. (1983) The distribution of deuterium and ^{18}O in dry soils: 1. Theory. *J. Hydrol.* **60**, 141–156.

Barnes C. J. and Allison G. B. (1988) Tracing of water movement in the unsaturated zone using stable isotopes of hydrogen and oxygen. *J. Hydrol.* **100**, 143–176.

Benettin P., Volkmann T. H. M., Von Freyberg J., Frentress J., Penna D., Dawson T. E. and Kirchner J. W. (2018) Effects of climatic seasonality on the isotopic composition of evaporating soil waters. *Hydrol. Earth Sys. Sci.***22**, 2881–2890.

Bergel S. J., Barkan E., Stein M. and Affek H. P. (2020) Carbonate ^{17}Oexcess as a paleo-hydrology proxy: Triple oxygen isotope fractionation between H_2O and biogenic aragonite, derived from freshwater mollusks. *Geochim. Cosmochim. Acta* **275**, 36-47.

Bernasconi S. M., Daëron M., Bergmann K. D., Bonifacie M., Meckler A. N., Affek H. P., Anderson, N., Bajnai D., Barkan E., Beverly E., Blamart D., Burgener L., Calmels D., Clog M., Davidheiser-Kroll B., Davies A., Dux F., Eiler J., Elliott B., Fetrow A.C., Fiebig J., Goldberg S., Hermoso M., Huntington K. W., Hyland E., Ingalls, M., Jaggi M., John C. M., Jost A. B., Katz S., Kelson J., Kluge T., Kocken I. J., Laskar, A., Leutert T. J., Liang D., Lucarelli J., Mackey T. J., Mangenot X., Meinicke N., Modestou S. E., Müller I. A., Murray S., Neary A., Packard N., Passey B. H., Pelletier E., Piasecki A., Schauer A., Snell K. E., Swart P. K., Tripati A., Upadhyay D., Vennemann T., Winkelstern I., Yarian D., Yoshida N., Zhang N. and Ziegler M. (2021) InterCarb: A community effort to improve inter-laboratory standardization of the carbonate clumped isotope thermometer using carbonate standards. *Geochem. Geophys. Geosystems* **22**, e2020GC009588.

Bershaw J., Penny S. M. and Garzione C. N. (2012) Stable isotopes of modern water across the Himalaya and eastern Tibetan Plateau: Implications for estimates of paleoelevation and paleoclimate. *J. Geophys. Res.* **117**, D02110.

Beverly E. J., Levin N. E., Passey B. H., Aron P. G., Yarian D. A., Page M. and Pelletier E. M. (2021) Triple oxygen and clumped isotopes in modern soil carbonate along an aridity gradient in the Serengeti, Tanzania. *Earth Planet. Sci. Lett.* **567**, 116952.

Bowen G. J., Fisher-Femal B., Reichart G.-J., Sluijs A. and Lear C. H. (2020) Joint inversion of proxy system models to reconstruct paleoenvironmental time series from heterogeneous data. *Clim. Past* **16**, 65-78.

Bowen G. J., Putman A., Brooks J. R., Bowling D. R., Oerter E. J. and Good S. P. (2018) Inferring the source of evaporated waters using stable H and O isotopes. *Oecologia* **187**, 1025–1039.

1099 Bowen G. J. and Revenaugh J. (2003) Interpolating the isotopic composition of modern meteoric
1100 precipitation. *Water Resour. Res.* **39**.

1101 Brand W., Assonov S. S. and Coplen T. B. (2010) Correction for the ^{17}O interference in $\delta^{13}C$
1102 measurements when analyzing CO_2 with stable isotope mass spectrometry (IUPAC
1103 Technical Report). *Pure Appl. Chem.* **82**, 1719–1733.

1104 Breecker D. O., Sharp Z. D. and McFadden L. D. (2010) Atmospheric CO2 concentrations
1105 during ancient greenhouse climates were similar to those predicted for A.D. 2100. *Proc.*
1106 *Natl. Acad. Sci. U.S.A.* **107**, 576–580.

1107 Breecker D. O., Sharp Z. D. and McFadden L. D. (2009) Seasonal bias in the formation and
1108 stable isotopic composition of pedogenic carbonate in modern soils from central New
1109 Mexico, USA. *Geol. Soc. Am. Bull.* **121**, 630–640.

1110 Brooks J. R., Barnard H. R., Coulombe R. and McDonnell J. J. (2010) Ecohydrologic separation
1111 of water between trees and streams in a Mediterranean climate. *Nat. Geosci.* **3**, 100–104.

1112 Broz A., Retallack G. J., Maxwell T. M. and Silva L. C. R. (2021) A record of vapour pressure
1113 deficit preserved in wood and soil across biomes. *Sci. Rep.* **11**, 1–12.

1114 Burgener L. K., Huntington K. W., Hoke G. D., Schauer A. J., Ringham M. C., Latorre C. and
1115 Díaz F. P. (2016) Variations in soil carbonate formation and seasonal bias over >4 km of
1116 relief in the western Andes (30°S) revealed by clumped isotope thermometry. *Earth*
1117 *Planet. Sci. Lett.* **441**, 188–199.

1118 Burgener L. K., Huntington K. W., Sletten R., Watkins J. M., Quade J. and Hallet B. (2018)
1119 Clumped isotope constraints on equilibrium carbonate formation and kinetic isotope
1120 effects in freezing soils. *Geochim. Cosmochim. Acta* **235**, 402–430.

1121 Caldwell M. M., Dawson T. E. and Richards J. H. (1998) Hydraulic Lift: Consequences of Water
1122 Efflux from the Roots of Plants. *Oecologia* **113**, 151–161.

1123 Cassel E. J., Smith M. E. and Jicha B. R. (2018) The Impact of Slab Rollback on Earth's
1124 Surface: Uplift and Extension in the Hinterland of the North American Cordillera.
1125 *Geophys. Res. Lett.* **45**, 10,996-11,004.

1126 Caves Rugenstein J. K. and Chamberlain C. P. (2018) The evolution of hydroclimate in Asia
1127 over the Cenozoic: A stable-isotope perspective. *Earth Sci. Rev.***185**, 1129–1156.

1128 Cerling T. E. (1992) Development of grasslands and savannas in East Africa during the
1129 Neogene. *Glob. Planet. Change* **5**, 241–247.

1130 Cerling T. E. (1984) The stable isotopic composition of modern soil carbonate and its relation to
1131 climate. *Earth Planet. Sci. Lett.* **71**, 229-240.

1132 Cerling T. E. and Quade J. (1993) Stable carbon and oxygen isotopes in soil carbonates.
1133 *Geophys. Monogr. Ser.* **78**, 217–231.

1134 Cerling T. E., Quade J., Wang Y. and Bowman J. R. (1989) Carbon isotopes in soils and
1135 palaeosols as ecology and palaeoecology indicators. *Nature* **341**, 138–139.

1136 Chamberlain C. P., Mix H. T., Mulch A., Hren M. T., Kent-Corson M. L., Davis S. J., Horton T.
1137 W. and Graham S. A. (2012) The cenozoic climatic and topographic evolution of the
1138 western north American Cordillera. *Am. J. Sci.* **312**, 213–262.

1139 Chamberlain C. P., Winnick M. J., Mix H. T., Chamberlain S. D. and Maher K. (2014) The
1140 impact of neogene grassland expansion and aridification on the isotopic composition of
1141 continental precipitation. *Global Biogeochem. Cycles* **28**, 992–1004.

1142 Cole D. R. and Monger H. C. (1994) Influence of atmospheric CO_2 on the decline of C_4 plants
1143 during the last deglaciation. *Nature* **368**, 533-535.

1144 Conant R. T., Dalla-Betta P., Klopatek C. C. and Klopatek J. M. (2004) Controls on soil
1145 respiration in semiarid soils. *Soil Biol. Biochem.* **36**, 945–951.

1146 Cotton J. M. and Sheldon N. D. (2012) New constraints on using paleosols to reconstruct
1147 atmospheric pCO 2. *Geol. Soc. Am. Bull.* **124**, 1411–1423.

1148 Craig H. and Gordon L. I. (1965) Deuterium and oxygen-18 variations in the ocean and the
1149 marine atmosphere. In *Stable Isotopes in Oceanographic Studies and Paleotemperatures*
1150 Spoleto, Italy.

1151 Criss R. E. (1999) *Principles of Stable Isotope Distribution*, Oxford University Press, USA.

1152 Daëron M., Blamart D., Peral M. and Affek H. P. (2016) Absolute isotopic abundance ratios and
1153 the accuracy of Δ_{47} measurements. *Chem. Geo.* **442**, 83–96.

1154 DeCelles P. G., Quade J., Kapp P., Fan M., Dettman D. L. and Ding L. (2007) High and dry in
1155 central Tibet during the Late Oligocene. *Earth Planet. Sci. Lett.* **253**, 389–401.

1156 Dee S., Emile-Geay J., Evans M. N., Allam A., Steig E. J. and Thompson D. M. (2016) PRYSM:
1157 An open-source framework for PRoxY System Modeling, with applications to oxygen-
1158 isotope systematics. *J. Adv. Model. Earth Syst.* **7**, 1220-1247.

1159 Defliese W. F., Hren M. T. and Lohmann K. C. (2015) Compositional and temperature effects of
1160 phosphoric acid fractionation on Δ_{47} analysis and implications for discrepant calibrations.
1161 *Chem. Geo.* **396**, 51–60.

1162 DePaolo D. J., Conrad M. E., Maher K. and Gee G. W. (2004) Evaporation Effects on Oxygen
1163 and Hydrogen Isotopes in Deep Vadose Zone Pore Fluids at Hanford, Washington.
1164 *Vadose Zone J.* **3**, 220–232.

1165 Deutz P., Montanez I. P. and Monger H. C. (2002) Morphology and stable and radiogenic
1166 isotope composition of pedogenic carbonates in late quaternary relict soils, New Mexico,
1167 U.S.A.: An integrated record of pedogenic overprinting. *J. Sediment. Res.* **72**, 809–822.

van Dijk J., Fernandez A., Bernasconi S. M., Rugenstein J. K. C., Passey S. R. and White T. (2020) Spatial pattern of super-greenhouse warmth controlled by elevated specific humidity. *Nat. Geosci.* **13,** 739-744.

Domínguez-Villar D., Bensa A., Švob M. and Krklec K. (2022) Causes and implications of the seasonal dissolution and precipitation of pedogenic carbonates in soils of karst regions – A thermodynamic model approach. *Geoderma* **423**, 115962.

Eagle R. A., Risi C., Mitchell J. L., Eiler J. M., Seibt U., Neelin J. D., Li G. and Tripati A. K. (2013) High regional climate sensitivity over continental China constrained by glacial-recent changes in temperature and the hydrological cycle. *Proc. Natl. Acad. Sci. U.S.A.* **110**, 8813–8.

Ehleringer J. R. and Dawson T. E. (1992) Water uptake by plants: perspectives from stable isotope composition. *Plant Cell Environ.* **15**, 1073–1082.

Eiler J. M. (2007) "Clumped-isotope" geochemistry—The study of naturally-occurring, multiply-substituted isotopologues. *Earth Planet. Sci. Lett.* **262**, 309–327.

Evans J. P., Smith R. B. and Oglesby R. J. (2004) Middle East climate simulation and dominant precipitation processes. *Int. J. Climatol.* **24**, 1671–1694.

Evans M. N., Tolwinski-Ward S. E., Thompson D. M. and Anchukaitis K. J. (2013) Applications of proxy system modeling in high resolution paleoclimatology. *Quat. Sci. Rev.* **76**, 16–28.

Evans N. P., Bauska T. K., Gázquez-Sánchez F., Brenner M., Curtis J. H. and Hodell D. A. (2018) Quantification of drought during the collapse of the classic Maya civilization. *Science* **361**, 498–501.

Evaristo J., Jasechko S. and McDonnell J. J. (2015) Global separation of plant transpiration from groundwater and streamflow. *Nature* **525**, 91–94.

Fan M., DeCelles P. G., Gehrels G. E., Dettman D. L., Quade J. and Peyton S. L. (2011) Sedimentology, detrital zircon geochronology, and stable isotope geochemistry of the lower Eocene strata in the Wind River Basin, central Wyoming. *Geol. Soc. Am. Bull.* **123**, 979–996.

Fick S. E. and Hijmans R. J. (2017) WorldClim 2: new 1-km spatial resolution climate surfaces for global land areas. *Int. J. Climatol.* **37**, 4302–4315.

Fiebig J., Bajnai D., Löffler N., Methner K., Krsnik E., Mulch A. and Hofmann S. (2019) Combined high-precision Δ48 and Δ47 analysis of carbonates. *Chem. Geo.* **522**, 186–191.

Fischer-Femal B. J. and Bowen G. J. (2021) Coupled carbon and oxygen isotope model for pedogenic carbonates. *Geochim. Cosmochim. Acta* **294**, 126–144.

Fosu B. R., Subba R., Peethambaran R., Bhattacharya S. K. and Ghosh P. (2020) Technical note: Developments and applications in triple oxygen isotope analysis of carbonates. *ACS Earth Space Chem.* **4**, 702–710.

Fox D. L. and Koch P. L. (2004) Carbon and oxygen isotopic variability in Neogene paleosol carbonates: constraints on the evolution of the C4-grasslands of the Great Plains, USA. *Palaeogeogr. Palaeoclimatol. Palaeoecol.***207**, 305–329.

Fox D. L. and Koch P. L. (2003) Tertiary history of C4 biomass in the Great Plains, USA. *Geology* **31**, 809–812.

Fricke H. C., Foreman B. Z. and Sewall J. O. (2010) Integrated climate model-oxygen isotope evidence for a North American monsoon during the Late Cretaceous. *Earth Planet. Sci. Lett.* **289**, 11–21.

Fricke H. C. and Wing S. L. (2004) Oxygen isotope and paleobotanical estimates of temperature and d18O - latitude gradients over North America during the Early Eocene. *Am. J. Sci..* **304**, 612–635.

Gallagher T. M., Hren M. T. and Sheldon N. D. (2019) The effect of soil temperature seasonality on climate reconstructions from Ppaleosols. *Am. J. Sci.* **319**, 549–581.

Gallagher T. M. and Sheldon N. D. (2016) Combining soil water balance and clumped isotopes to understand the nature and timing of pedogenic carbonate formation. *Chem. Geo.* **435**, 79–91.

Garzione C. N., Hoke G. D., Libarkin J. C., Withers S., MacFadden B., Eiler J. M., Ghosh P. and Mulch A. (2008) Rise of the Andes. *Science* **320**, 1304–7.

Gazis C. and Feng X. (2004) A stable isotope study of soil water: evidence for mixing and preferential flow paths. *Geoderma* **119**, 97–111.

Gázquez F., Morellón M., Bauska T., Herwartz D., Surma J., Moreno A., Staubwasser M., Valero-Garcés B., Delgado-Huertas A. and Hodell D. A. (2018) Triple oxygen and hydrogen isotopes of gypsum hydration water for quantitative paleo-humidity reconstruction. *Earth Planet. Sci. Lett.* **481**, 177–188.

Gibson J. J., Birks S. J. and Edwards T. W. D. (2008) Global prediction of δ_A and δ^2H-$\delta^{18}O$ evaporation slopes for lakes and soil water accounting for seasonality. *Global Biogeochem. Cycles* **22,** GB2031.

Gile L. H., Peterson F. F. and Grossman R. B. (1966) Morphological and Genetic Sequences of Carbonate Accumulation in Desert Soils. *Soil Sci.* **101**, 347–360.

Giménez R., Bartolomé M., Gázquez F., Iglesias M. and Moreno A. (2021) Underlying climate controls in triple oxygen (^{16}O, ^{17}O, ^{18}O) and Hydrogen (^{1}H, ^{2}H) Isotopes Composition of Rainfall (Central Pyrenees). *Front. Earth Sci.* **9**, 633698.

Guo W. (2020) Kinetic clumped isotope fractionation in the DIC-H_2O-CO_2 system: Patterns, controls, and implications. *Geochim. Cosmochim. Acta* **268**, 230–257.

Guo W. and Zhou C. (2019) Triple Oxygen Isotope Fractionation in the DIC-H_2O-CO_2 system: A Numerical Framework and Its Implications. *Geochim. Cosmochim. Acta* **246**, 541–564.

Havranek R. E., Snell K. E., Davidheiser-Kroll B., Bowen G. J. and Vaughn B. (2020) The Soil Water Isotope Storage System (SWISS): An integrated soil water vapor sampling and multiport storage system for stable isotope geochemistry. *Rapid Comm. Mass Spectrom.* **34**, e8783.

Herwartz D., Surma J., Voigt C., Assonov S. and Staubwasser M. (2017) Triple oxygen isotope systematics of structurally bonded water in gypsum. *Geochim. Cosmochim. Acta* **209**, 254-266.

Hoke G. D., Garzione C. N., Araneo D. C., Latorre C., Strecker M. R. and Williams K. J. (2009) The stable isotope altimeter: Do Quaternary pedogenic carbonates predict modern elevations? *Geology* **37**, 1015–1018.

Hoke G. D., Liu-Zeng J., Hren M. T., Wissink G. K. and Garzione C. N. (2014) Stable isotopes reveal high southeast Tibetan Plateau margin since the Paleogene. *Earth Planet. Sci. Lett.* **394**, 270–278.

Hough B. G., Fan M. and Passey B. H. (2014) Calibration of the clumped isotope geothermometer in soil carbonate in Wyoming and Nebraska, USA: Implications for paleoelevation and paleoclimate reconstruction. *Earth Planet. Sci. Lett.* **391**.

Hsieh J. C. C., Chadwick O. A., Kelly E. F. and Savin S. M. (1998) Oxygen isotopic composition of soil water: Quantifying evaporation and transpiration. *Geoderma* **82**, 269–293.

Huntington K. W. and Petersen S. V. (2023) Frontiers of Carbonate Clumped Isotope Thermometry. *Annu. Rev. Earth Planet. Sci.* **51**, 611-641.

Huth T. E., Cerling T. E., Marchetti D. W., Bowling D. R., Ellwein A. L. and Passey B. H. (2019) Seasonal bias in soil carbonate formation and its implications for interpreting high-resolution paleoarchives: evidence from southern Utah. *J. Geophys. Res. Biogeosci.* **124**, 616–632.

Huth T. E., Passey B. H., Cole J. E., Lachniet M. S., McGee D., Denniston R. F., Truebe S. and Levin N. E. (2022) A framework for triple oxygen isotopes in speleothem paleoclimatology. *Geochim. Cosmochim. Acta* **319**, 191–219.

Ibarra D. E., Kukla T., Methner K., Mulch A. and Chamberlain C. P. (2021) Reconstructing past elevations from triple oxygen isotopes of lacustrine chert: Application to the Eocene Nevadaplano, Elko Basin, Nevada, United States. *Front. Earth Sci.* **9**, 628868.

Ji S., Nie J., Breecker D. O., Luo Z. and Song Y. (2017) Intensified aridity in northern China during the middle Piacenzian warm period. *J. Asian Earth Sci.* **147**, 222–225.

Jones M. M., Petersen S. V. and Curley A. N. (2022) A tropically hot mid-Cretaceous North American Western Interior Seaway. *Geology* **50**, 954–958.

Katz S. A., Levin N. E., Rodbell D. T., Gillikin D. P., Aron P. G., Passey B. H., Tapia P. M., Serrepe A. R. and Abbott M. B. (2023) Detecting hydrologic distinctions among Andean lakes using clumped and triple oxygen isotopes. *Earth Planet. Sci. Lett.* **602**, 117927.

Kebede S., Charles K., Godfrey S., MacDonald A. and Taylor R. G. (2021) Regional-scale interactions between groundwater and surface water under changing aridity: evidence from the River Awash Basin, Ethiopia. *Hydrol. Sci. J.* **66**, 450–463.

Kelson J. R., Huntington K. W., Breecker D. O., Burgener L. K., Gallagher T. M., Hoke G. D. and Petersen S. V. (2020) A proxy for all seasons? A synthesis of clumped isotope data from Holocene soil carbonates. *Quat. Sci. Rev.* **234**, 106259.

Kelson J. R., Petersen S. V., Niemi N. A., Passey B. H. and Curley A. N. (2022) Looking upstream with clumped and triple oxygen isotopes of estuarine oyster shells in the early Eocene of California, USA. *Geology* **50**, 755-759.

Kelson J. R., Watford D., Bataille C. P., Huntington K. W., Hyland E. G. and Bowen G. J. (2018) Warm terrestrial subtropics during the Paleocene and Eocene: Carbonate clumped isotope (Δ47) evidence from the Tornillo Basin, Texas (USA). *Paleoceanogr. Paleoclimatol.*, **33**, 1230-1249.

Kim S. T. and O'Neil J. R. (1997) Equilibrium and nonequilibrium oxygen isotope effects in synthetic carbonates. *Geochim. Cosmochim. Acta* **61**, 3461–3475.

Kleinert K. and Strecker M. R. (2001) Climate change in response to orographic barrier uplift: Paleosol and stable isotope evidence from the late Neogene Santa María basin, northwestern Argentina. *Geol. Soc. Am. Bull.* **113**, 728–742.

Kovda I. (2020) Vertisols: Extreme features and extreme environment. *Geoderma Reg.* **22**, e00312.

Kovda I., Mora C. I. and Wilding L. P. (2006) Stable isotope compositions of pedogenic carbonates and soil organic matter in a temperate climate Vertisol with gilgai, southern Russia. *Geoderma* **136**, 423–435.

Kukla T., Rugenstein J. K. C., Ibarra D. E., Winnick M. J., Strömberg C. a. E. and Chamberlain C. P. (2022) Drier winters drove Cenozoic open habitat expansion in North America. *AGU Advances* **3**, e2021AV000566.

Kukla T., Winnick M. J., Maher K., Ibarra D. E. and Chamberlain C. P. (2019) The sensitivity of terrestrial $\delta^{18}O$ gradients to hydroclimate evolution. *J. Geophys. Res. Atmos.* **124**, 563–582.

1307 Landais A., Barkan E., Yakir D. and Luz B. (2006) The triple isotopic composition of oxygen in
1308 leaf water. *Geochim. Cosmochim. Acta* **70**, 4105–4115.

1309 Landais A., Risi C., Bony S., Vimeux F., Descroix L., Falourd S. and Bouygues A. (2010)
1310 Combined measurements of ^{17}Oexcess and d-excess in African monsoon precipitation:
1311 Implications for evaluating convective parameterizations. *Earth Planet. Sci. Lett.* **298**,
1312 104–112.

1313 Lehmann S. B., Levin N. E., Passey B. H., Hu H., Cerling T. E., Miller J. H., Arppe L., Beverly
1314 E. J., Hoppe K. A., Huth T. E., Kelson J. R., Luyt J. and Sealy J. (2022) Triple oxygen
1315 isotope distribution in modern mammal teeth and potential geologic applications.
1316 *Geochim. Cosmochim. Acta* **331**, 105–122.

1317 Levin N. E., Brown F. H., Behrensmeyer A. K., Bobe R. and Cerling T. E. (2011) Paleosol
1318 carbonates from the Omo Group: Isotopic records of local and regional environmental
1319 change in east africa. *Palaeogeogr. Palaeoclimatol. Palaeoecol.***307**, 75–89.

1320 Levin N. E., Quade J., Simpson S. W., Semaw S. and Rogers M. (2004) Isotopic evidence for
1321 Plio–Pleistocene environmental change at Gona, Ethiopia. *Earth Planet. Sci. Lett.* **219**,
1322 93–110.

1323 Levin N. E., Zipser E. J. and Ceding T. E. (2009) Isotopic composition of waters from Ethiopia
1324 and Kenya: Insights into moisture sources for eastern Africa. *J. Geophys. Res. Atmos.*
1325 **114**, 1–13.

1326 Li L. and Garzione C. N. (2017) Spatial distribution and controlling factors of stable isotopes in
1327 meteoric waters on the Tibetan Plateau: Implications for paleoelevation reconstruction.
1328 *Earth Planet. Sci. Lett.* **460**, 302–314.

1329 Li S., Levin N. E. and Chesson L. A. (2015) Continental scale variation in ^{17}O-excess of
1330 meteoric waters in the United States. *Geochim. Cosmochim. Acta* **164**, 110–126.

1331 Li S., Levin N. E., Soderberg K., Dennis K. J. and Caylor K. K. (2017) Triple oxygen isotope
1332 composition of leaf waters in Mpala, central Kenya. *Earth Planet. Sci. Lett.* **468**, 38–50.

1333 Licht A., Kelson J., Bergel S., Schauer A., Petersen S. V., Capirala A., Huntington K. W.,
1334 Dupont-Nivet G., Win Z. and Aung D. W. (2022) Dynamics of Pedogenic Carbonate
1335 Growth in the Tropical Domain of Myanmar. *Geochem. Geophys. Geosystems* **23**,
1336 e2021GC009929.

1337 Licht A., Quade J., Kowler A., De Los Santos M., Hudson A. M., Schauer A. J., Huntington K.
1338 W., Copeland P. and Lawton T. F. (2017) Impact of the North American monsoon on
1339 isotope paleoaltimeters: Implications for the paleoaltimetry of the American southwest.
1340 *Am. J. Sci.* **317**, 1–33.

1341 Liu B., Phillips F., Hoines S., Campbell A. R. and Sharma P. (1995) Water movement in desert
1342 soil traced by hydrogen and oxygen isotopes, chloride, and chlorine-36, southern
1343 Arizona. *J. Hydrol.* **168**, 91–110.

1344 Liu B., Phillips F., and Campbell A. R. (1996) Stable carbon and oxygen isotopes of pedogenic
1345 carbonates, Ajo Mountains, southern Arizona: implications for paleoenvironmental
1346 change. *Palaeogeogr. Palaeoclimatol. Palaeoecol.***124**, 233–246.

1347 Luz B. and Barkan E. (2010) Variations of $^{17}O/^{16}O$ and $^{18}O/^{16}O$ in meteoric waters. *Geochim.*
1348 *Cosmochim. Acta* **74**, 6276–6286.

1349 Mathieu R. and Bariac T. (1996) A numerical model for the simulation of stable isotope profiles
1350 in drying soils. *J. Geophys. Res. Atmos.* **101**, 12685–12696.

1351 McDonald, E.V. McFadden, L.D. and Wells, S.G., 2003, Regional response of alluvial fans to
1352 the Pleistocene-Holocene climatic transition, Mojave Desert, California, in Enzel, Y.,
1353 Wells, S.G., and Lancaster, N., (Eds.), Paleoenvironments and paleohydrology of the
1354 Mojave and southern Great Basin Deserts: Boulder, Colorado, Geological Society of
1355 America Special Paper 368, p. 189–205.
1356
1357 Methner K., Mulch A., Fiebig J., Wacker U., Gerdes A., Graham S. A. and Chamberlain C. P.
1358 (2016) Rapid Middle Eocene temperature change in western North America. *Earth*
1359 *Planet. Sci. Lett.* **450**, 132–139.

1360 Meyer N. A., Breecker D. O., Young M. H. and Litvak M. E. (2014) Simulating the Effect of
1361 Vegetation in Formation of Pedogenic Carbonate. *Soil Sci. Soc. Am. J.* **78**, 914.

1362 Miller D. L., Mora C. I. and Driese S. G. (2007) Isotopic variability in large carbonate nodules in
1363 Vertisols: Implications for climate and ecosystem assessments. *Geoderma* **142**, 104–111.

1364 Mintz J. S., Driese S. G., Breecker D. O. and Ludvigson G. A. (2011) Influence of Changing
1365 Hydrology on Pedogenic Calcite Precipitation in Vertisols, Dance Bayou, Brazoria
1366 County, Texas, U.S.A.: Implications for Estimating Paleoatmospheric PCO2. *J.*
1367 *Sediment. Res.* **81**, 394–400.

1368 Monger H. C., Cole D. R., Gish J. W. and Giordano T. H. (1998) Stable carbon and oxygen
1369 isotopes in Quaternary soil carbonates as indicators of ecogeomorphic changes in the
1370 northern Chihuahuan Desert, USA. *Geoderma* **82**, 137–172.

1371 Montañez I. P. (2013) Modern soil system constraints on reconstructing deep-time atmospheric
1372 CO2. *Geochim. Cosmochim. Acta* **101**, 57–75.

1373 Mulch A. (2016) Stable isotope paleoaltimetry and the evolution of landscapes and life. *Earth*
1374 *Planet. Sci. Lett.* **433**, 180–191.

1375 Mulch A., Chamberlain C. P., Cosca M. A., Teyssier C., Methner K., Hren M. T. and Graham S.
1376 A. (2015) Rapid change in high-elevation precipitation patterns of western North
1377 America during the Middle Eocene Climatic Optimum (MECO). *Am. J. Sci.* **315**, 317–
1378 336.

1379 Nordt L. C., Atchley S. C. and Dworkin S. I. (2003) Terrestrial evidence for two greenhouse
1380 events in the latest Cretaceous. *Geol. Soc. Am. Today* **13**, 4–9.

1381 Nordt L. C., Wilding L. P., Lynn W. C. and Crawford C. C. (2004) Vertisol genesis in a humid
1382 climate of the coastal plain of Texas, U.S.A. *Geoderma* **122**, 83–102.

1383 Oerter E. J. and Amundson R. G. (2016) Climate controls on spatial temporal variations in the
1384 formation of pedogenic carbonate in the western Great Basin of North America. *Geol.*
1385 *Soc. Am. Bull.* **128**, 1095–1104.

1386 Oerter E. J. and Bowen G. (2017) In situ monitoring of H and O stable isotopes in soil water
1387 reveals ecohydrologic dynamics in managed soil systems. *Ecohydrology* **10**, 1–13.

1388 Oerter E. J. and Bowen G. J. (2019) Spatio-temporal heterogeneity in soil water stable isotopic
1389 composition and its ecohydrologic implications in semiarid ecosystems. *Hydrol. Process.*
1390 **33**, 1724–1738.

1391 Oerter E. J., Sharp W. D., Oster J. L., Ebeling A., Valley J. W., Kozdon R., Orland I. J.,
1392 Hellstrom J., Woodhead J. D., Hergt J. M., Chadwick O. A. and Amundson R. (2016)
1393 Pedothem carbonates reveal anomalous North American atmospheric circulation 70,000-
1394 55,000 years ago. *Proc. Natl. Acad. Sci. U.S.A.* **113**, 919–924.

1395 O'Hora H. E., Petersen S. V., Vellekoop J., Jones M. M. and Scholz S. R. (2022) Clumped-
1396 isotope-derived climate trends leading up to the end-Cretaceous mass extinction in
1397 northwestern Europe. *Clim. Past* **18**, 1963–1982.

1398 Pack A., Gehler A. and Süssenberger A. (2013) Exploring the usability of isotopically
1399 anomalous oxygen in bones and teeth as paleo-CO2-barometer. *Geochim. Cosmochim.*
1400 *Acta* **102**, 306–317.

1401 Passey B. H., Hu H., Ji H., Montanari S., Li S., Henkes G. A. and Levin N. E. (2014) Triple
1402 oxygen isotopes in biogenic and sedimentary carbonates. *Geochim. Cosmochim. Acta*
1403 **141**, 1–25.

1404 Passey B. H. and Ji H. (2019) Triple oxygen isotope signatures of evaporation in lake waters and
1405 carbonates: A case study from the western United States. *Earth Planet. Sci. Lett.* **518**, 1–
1406 12.

1407 Passey B. H. and Levin N. E. (2021) Triple oxygen isotopes in meteoric waters, carbonates,
1408 biological apatites: Implications for continental paleoclimate reconstruction. *Rev.*
1409 *Mineral. Geochem.* **86**, 429-462.

1410 Pendall E. G., Harden J. W., Trumbore S. E. and Chadwick O. A. (1994) Isotopic approach to
1411 soil carbonate dynamics and implications for paleoclimatic interpretations. *Quaternary*
1412 *Research* **42**, 60–71.

1413 Peters N. A., Huntington K. W. and Hoke G. D. (2013) Hot or not? Impact of seasonally variable
1414 soil carbonate formation on paleotemperature and O-isotope records from clumped
1415 isotope thermometry. *Earth Planet. Sci. Lett.* **361**, 208–218.

Petersen S. V., Defliese W. F., Saenger C., Daëron M., Huntington K. W., John C. M., Kelson J. R., Bernasconi S. M., Colman A. S., Kluge T., Olack G. A., Schauer A. J., Bajnai D., Bonifacie M., Breitenbach S. F. M., Fiebig J., Fernandez A. B., Henkes G. A., Hodell D., Katz A., Kele S., Lohmann K. C., Passey B. H., Peral M. Y., Petrizzo D. A., Rosenheim B. E., Tripati A., Venturelli R., Young E. D. and Winkelstern I. Z. (2019) Effects of improved ^{17}O Correction on interlaboratory agreement in clumped isotope calibrations, estimates of mineral-specific offsets, and temperature dependence of acid digestion fractionation. *Geochem. Geophys. Geosystems* **20**, 3495–3519.

Poage M. A. and Chamberlain C. P. (2001) Empirical relationships between elevation and the stable isotopic composition of precipitation and surface waters: Considerations for studies of paleoelevation change. *Am. J. Sci.* **301**, 1–15.

Quade J., Cerling T. E. and Bowman J. R. (1989) Systematic variations in the carbon and oxygen isotopic composition of pedogenic carbonate along elevation transects in the southern Great Basin, United States. *Geol. Soc. Am. Bull.* **101**, 464–475.

Quade J., Eiler J. M., Daëron M. and Achyuthan H. (2013) The clumped isotope geothermometer in soil and paleosol carbonate. *Geochim. Cosmochim. Acta* **105**, 92–107.

Quade J., Garzione C. N. and Eiler J. M. (2007a) Paleoelevation reconstruction using pedogenic carbonates. *Rev. Mineral. Geochem.* **66**, 53–87.

Quade J., Rech J. A., Latorre C., Betancourt J. L., Gleeson E. and Kalin M. T. K. (2007b) Soils at the hyperarid margin: The isotopic composition of soil carbonate from the Atacama Desert, Northern Chile. *Geochim. Cosmochim. Acta* **71**, 3772–3795.

Railsback L. B. (2021) Pedogenic carbonate nodules from a forested region of humid climate in central Tennessee, USA, and their implications for interpretation of C_3-C_4 relationships and seasonality of meteoric precipitation from carbon isotope ($\delta^{13}C$) data. *Catena* **200**, 1–8.

Rech J. A., Currie B. S., Jordan T. E., Riquelme R., Lehmann S. B., Kirk-Lawlor N. E., Li S. and Gooley J. T. (2019) Massive middle Miocene gypsic paleosols in the Atacama Desert and the formation of the Central Andean rain-shadow. *Earth Planet. Sci. Lett.* **506**, 184–194.

Retallack G. J. (2005) Pedogenic carbonate proxies for amount and seasonality of precipitation in paleosols. *Geology* **33**, 333–336.

Ringham M. C., Hoke G. D., Huntington K. W. and Aranibar J. N. (2016) Influence of vegetation type and site-to-site variability on soil carbonate clumped isotope records, Andean piedmont of Central Argentina (32–34°S). *Earth Planet. Sci. Lett.* **440**, 1–11.

Risi C., Landais A., Winkler R. and Vimeux F. (2013) Can we determine what controls the spatio-temporal distribution of d-excess and ^{17}O-excess in precipitation using the LMDZ general circulation model? *Clim. Past* **9**, 2173–2193.

Rowley D. B. (2007) Stable isotope-based paleoaltimetry: Theory and validation. *Rev. Mineral. Geochem.* **66**, 23–52.

Schauer A. J., Kelson J. R., Saenger C. and Huntington K. W. (2016) Choice of ^{17}O correction affects clumped isotope (Δ_{47}) values of CO_2 measured with mass spectrometry. *Rapid Comm. Mass Spectrom.* **30**, 2607–2616.

Schoenemann S. W., Schauer A. J. and Steig E. J. (2013) Measurement of SLAP2 and GISP $\delta^{17}O$ and proposed VSMOW-SLAP normalization for $\delta^{17}O$ and ^{17}Oexcess. *Rapid Comm. Mass Spectrom.* **27**, 582–590.

Sengupta S., Peters S. T. M., Reitner J., Duda J. P. and Pack A. (2020) Triple oxygen isotopes of cherts through time. *Chem. Geo.* **554**, 119789.

Sharp Z. D. and Wostbrock J. A. G. (2021) Standardization for the triple oxygen isotope system: Waters, silicates, carbonates, air, and sulfates. *Rev. Mineral. Geochem.* **86**, 179–196.

Sharp Z. D., Wostbrock J. A. G. and Pack A. (2018) Mass-dependent triple oxygen isotope variations in terrestrial materials. *Geochem. Perspect. Lett.* **7**, 27–31.

Shi P., Huang Y., Ji W., Xiang W., Evaristo J. and Li Z. (2021) Impacts of deep-rooted fruit trees on recharge of deep soil water using stable and radioactive isotopes. *Agric. For. Meteorol.* **300**, 108325.

Smith G. A., Wang Y., Cerling T. E. and Geissman J. W. (1993) Comparison of a paleosol-carbonate isotope record to other records of Pliocene-early Pleistocene climate in the western United States. *Geology* **21**, 691–694.

Snell K. E., Thrasher B. L., Eiler J. M., Koch P. L., Sloan L. C. and Tabor N. J. (2013) Hot summers in the Bighorn Basin during the early Paleogene. *Geology* **41**, 55–58.

Song B., Zhang K., Zhang L., Ji J., Hong H., Wei Y., Xu Y., Algeo T. J. and Wang C. (2018) Qaidam Basin paleosols reflect climate and weathering intensity on the northeastern Tibetan Plateau during the Early Eocene Climatic Optimum. *Palaeogeogr. Palaeoclimatol. Palaeoecol.* **512**, 6–22.

Sprenger M. and Allen S. T. (2020) What ecohydrologic separation is and where we can go with it. *Water Resour. Res.* **56**, e2020WR027238.

Sprenger M., Leistert H., Gimbel K. and Weiler M. (2016) Illuminating hydrological processes at the soil-vegetation-atmosphere interface with water stable isotopes. *Rev. Geophys.* **545**, 674–704.

Sprenger M., Tetzlaff D., Buttle J., Carey S. K., Mcnamara J. P., Laudon H., Shatilla N. J., Soulsby C., Buttle J., Carey S. K., Shatilla N. J. and Soulsby C. (2018) Storage, mixing, and fluxes of water in the critical zone across northern environments inferred by stable isotopes of soil water. *Hydrol. Process.* **32**, 1720–1737.

1487 Sprenger M., Tetzlaff D. and Soulsby C. (2017) Soil water stable isotopes reveal evaporation
1488 dynamics at the soil–plant–atmosphere interface of the critical zone. *Hydrol. Earth Sys.*
1489 *Sci.***21**, 3839–3858.

1490 Surma J., Assonov S., Bolourchi M. J. and Staubwasser M. (2015) Triple oxygen isotope
1491 signatures in evaporated water bodies from the Sistan Oasis, Iran. *Geophys. Res. Lett.* **42**,
1492 8456–8462.

1493 Surma J., Assonov S. S., Herwartz D., Voigt C. and Staubwasser M. (2018) The evolution of
1494 ^{17}O-excess in surface water of the arid environment during recharge and evaporation. *Sci.*
1495 *Rep.* **8**, 4972.

1496 Surma J., Assonov S. and Staubwasser M. (2021) Triple oxygen isotope systematics in the
1497 hydrologic cycle. *Rev. Mineral. Geochem.* **86**, 401–428.

1498 Tabor N. J., Myers T. S., Gulbranson E., Rasmussen C. and Sheldon N. D. (2013) Carbon stable
1499 isotope composition of modern calcareous soil profiles in California: Implications for
1500 CO_2 reconstructions from calcareous paleosols. In: Driese, S.G. (Ed.), New Frontiers in
1501 Paleopedology and Terrestrial Paleoclimatology: Paleosols and Soil Surface Analog
1502 Systems, Society for Sedimentary Geology Special Publication **104**, 17–34.

1503 Takeuchi A., Goodwin A. J., Moravec B. G., Larson P. B. and Keller C. K. (2009) Isotopic
1504 evidence for temporal variation in proportion of seasonal precipitation since the last
1505 glacial time in the inland Pacific Northwest of the USA. *Quat. Res.* **72**, 198–206.

1506 Uchikawa J. and Zeebe R. E. (2012) The effect of carbonic anhydrase on the kinetics and
1507 equilibrium of the oxygen isotope exchange in the CO_2–H_2O system: Implications for
1508 $\delta^{18}O$ vital effects in biogenic carbonates. *Geochim. Cosmochim. Acta* **95**, 15–34.

1509 Voarintsoa N. R. G., Barkan E., Bergel S., Vieten R. and Affek H. P. (2020) Triple oxygen
1510 isotope fractionation between $CaCO_3$ and H_2O in inorganically precipitated calcite and
1511 aragonite. *Chem. Geo.* **539**, 119500.

1512 Voigt C., Herwartz D., Dorador C. and Staubwasser M. (2021) Triple oxygen isotope
1513 systematics of evaporation and mixing processes in a dynamic desert lake system.
1514 *Hydrol. Earth Sys. Sci.* **25**, 1211–1228.

1515 Voigt, C., Alexandre, A., Reiter, I.M., Orts, J., Vallet-Coulomb, C., Piel, C., Mazur, J., Aleman,
1516 J.C., Sonzogni, C., Miche, H., Ogée, J. (2023). Examination of the parameters controlling
1517 the triple oxygen isotope composition of grass leaf water and phytoliths at a
1518 Mediterranean site: a model–data approach. *Biogeosciences* **20**, 2161-2187.

1519 Wang Y., McDonald E. V., Amundson R. G., McFadden L. D. and Chadwick O. A. (1996) An
1520 isotopic study of soils in chronological sequences of alluvial deposits, Providence
1521 Mountains, California. *Geol. Soc. Am. Bull.* **108**, 379–391.

1522 Winnick M. J., Chamberlain C. P., Caves J. K. and Welker J. M. (2014) Quantifying the isotopic
1523 "continental effect." *Earth Planet. Sci. Lett.* **406**, 123–133.

Winnick M. J., Welker J. M. and Chamberlain C. P. (2013) Stable isotopic evidence of El Niño-like atmospheric circulation in the Pliocene western United States. *Clim. Past* **9**, 903–912.

Wostbrock J. A. G., Brand U., Coplen T. B., Swart P. K., Carlson S. J., Brearley A. J. and Sharp Z. D. (2020a) Calibration of carbonate-water triple oxygen isotope fractionation: seeing through diagenesis in ancient carbonates. *Geochim. Cosmochim. Acta* **288**, 369–388.

Wostbrock J. A. G., Cano E. J. and Sharp Z. D. (2020b) An internally consistent triple oxygen isotope calibration of standards for silicates, carbonates and air relative to VSMOW2 and SLAP2. *Chem. Geo.* **533**, 119432.

Xia Z. (2023) Quantifying the Fingerprint of Oceanic Moisture Source Conditions in Deuterium and ^{17}O Excess Parameters of Precipitation. *Geophys. Res. Lett.* **50**, e2022GL101901.

Xia Z., Surma J. and Winnick M. J. (2023) The response and sensitivity of deuterium and ^{17}O excess parameters in precipitation to hydroclimate processes. *Earth Sci. Rev.* **242**, 104432.

Young E. D., Galy A. and Nagahara H. (2002) Kinetic and equilibrium mass-dependent isotope fractionation laws in nature and their geochemical and cosmochemical significance. *Geochim. Cosmochim. Acta* **66**, 1095–1104.

Zamanian K., Pustovoytov K. and Kuzyakov Y. (2016) Pedogenic carbonates: Forms and formation processes. *Earth Sci. Rev.***157**, 1–17.

Zhou J. and Chafetz H. S. (2010) Pedogenic carbonates in Texas: Stable-isotope distributions and their implications for reconstructing region-wide paleoenvironments. *J. Sediment. Res.* **80**, 137–150.

Zhou T., Šimůnek J. and Braud I. (2021) Adapting HYDRUS-1D to simulate the transport of soil water isotopes with evaporation fractionation. *Environ. Model. Softw.* **143**, 105118.

Zhu J., Poulsen C. J., Otto-Bliesner B. L., Liu Z., Brady E. C. and Noone D. C. (2020) Simulation of early Eocene water isotopes using an Earth system model and its implication for past climate reconstruction. *Earth Planet. Sci. Lett.* **537**, 116164.

Zimmerman, Ehhaldt, and Munnich (1967) Soil-water movement and evapotranspiration: Changes in the isotopic composition of water. In *Isotopes and Hydrology* International Atomic Energy Agency, Vienna, Austria. pp. 567–586.

Zomer R. J., Xu J. and Trabucco A. (2022) Version 3 of the Global Aridity Index and Potential Evapotranspiration Database. *Sci. Data* **9**, 409.

Figures

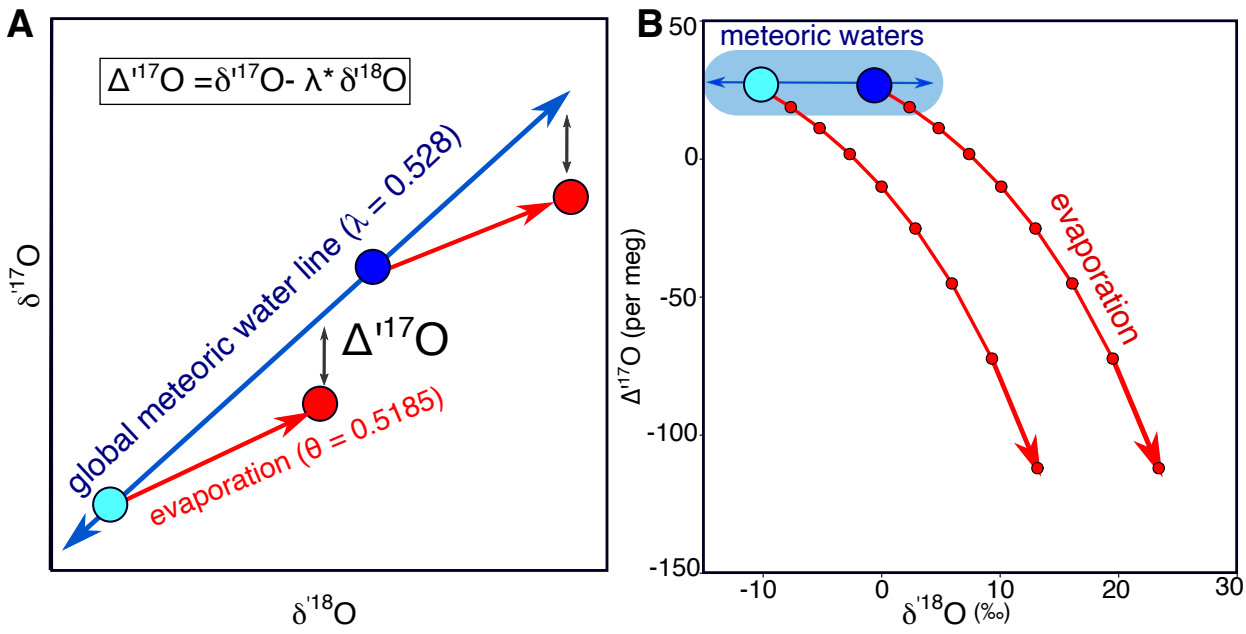

Figure 1: Schematic representation of the definition of $\Delta'^{17}O$ and the evolution of $\Delta'^{17}O$ and $\delta'^{18}O$ during evaporation. A) Schematic of $\delta'^{18}O$ vs $\delta'^{17}O$ visually defining $\Delta'^{17}O$. Progressive evaporation, a kinetic process, will cause $\delta'^{18}O$ and $\delta'^{17}O$ to evolve along a shallower slope than the reference slope, which is defined by typical meteoric waters. B) Evaporation leads to higher $\delta'^{18}O$ values and lower $\Delta'^{17}O$ values in remaining water. The red lines represent progressive evaporation from waters that start with distinct $\delta'^{18}O$ values. $\Delta'^{17}O$ is not sensitive to the initial $\delta'^{18}O$ value. The evaporation trajectory shown is for the water remaining during pan evaporation at a relative humidity of 0.4, ${}^{18}\alpha_{diff}$ of 1.0142, with the fraction of remaining water marked in

increments of 0.1 (modified from example in Passey and Levin, (2021), equations of Criss, (1999)).

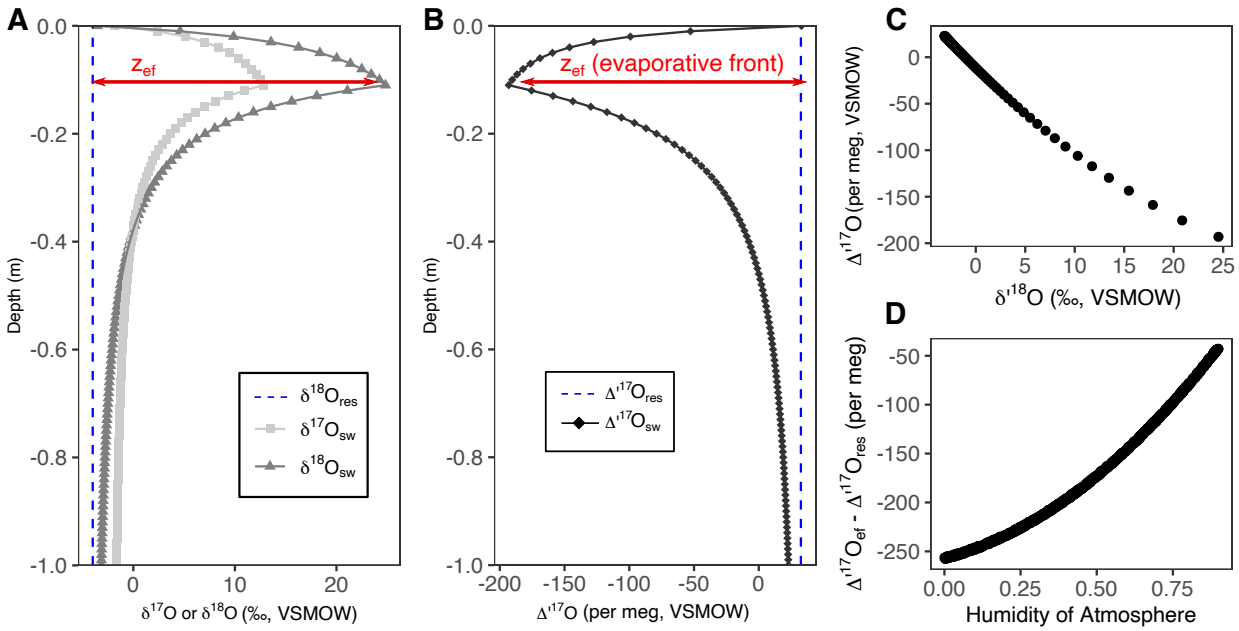

Figure 2: Predicted isotopic composition of soil water in steady state.

A and B) Predicted $\delta^{18}O$, $\delta^{17}O$ and $\Delta'^{17}O$ of soil water with depth in a steady-state soil profile, calculated using a single set of typical parameters (given in Table S1) (θ_{diff} = 0.5185). Vertical blue dashed line indicates the isotopic composition of the water in the soil pores, the 'reservoir.' C) The $\delta'^{18}O$-$\Delta'^{17}O$ relationship for the same set of typical parameters. This set of parameters yields a $\delta'^{18}O$-$\Delta'^{17}O$ trend of -8.7 per meg/‰, equivalent to a slope in $\delta'^{18}O$-$\delta'^{17}O$ of 0.5193 (i.e., λ_{soil}) D) Possible values of the isotopic offset between $\Delta'^{17}O$ at the evaporative front and the reservoir water, varying model parameters in 1000 simulations. The humidity of the overlying atmosphere is a strong control on the maximum isotopic offset. The sensitivity of $\delta'^{18}O$ and $\Delta'^{17}O$ to other variables is described in the Supplementary Material (Figures S1-S3).

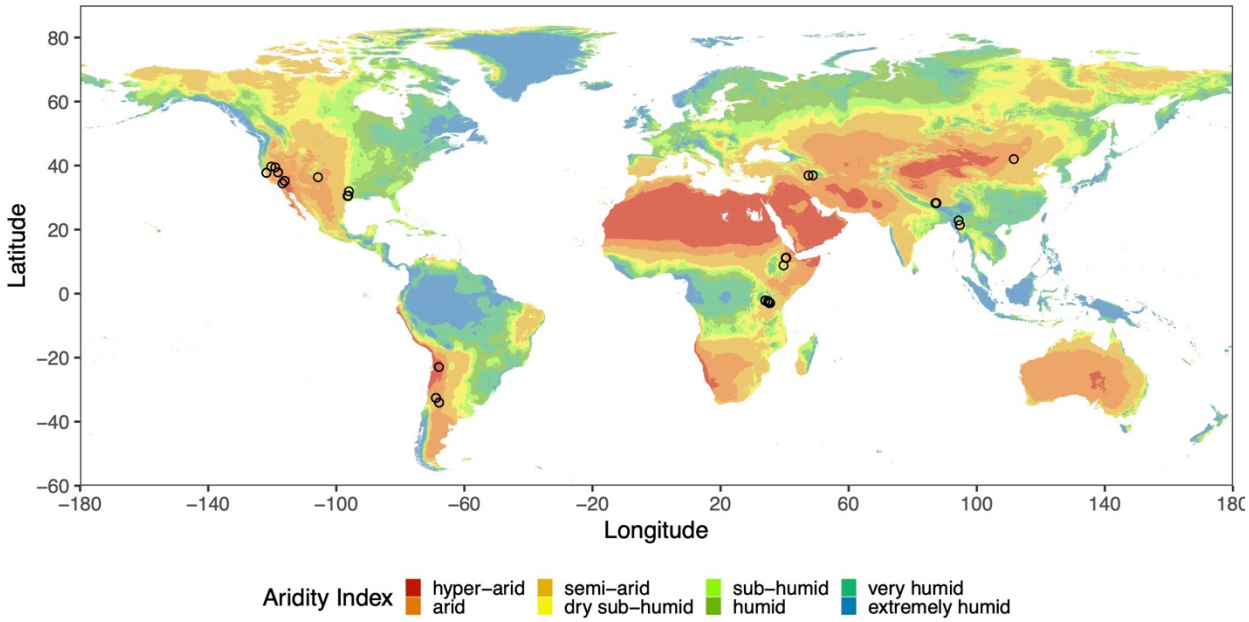

1586

1587 **Figure 3: Locations of pedogenic carbonate samples considered in this study**. Study sites are

1588 indicated with unfilled black circles. The AI is from World Clim 2 Data (Fick and Hijmans,

1589 2017); down sampled from 30 arc second data.

1590

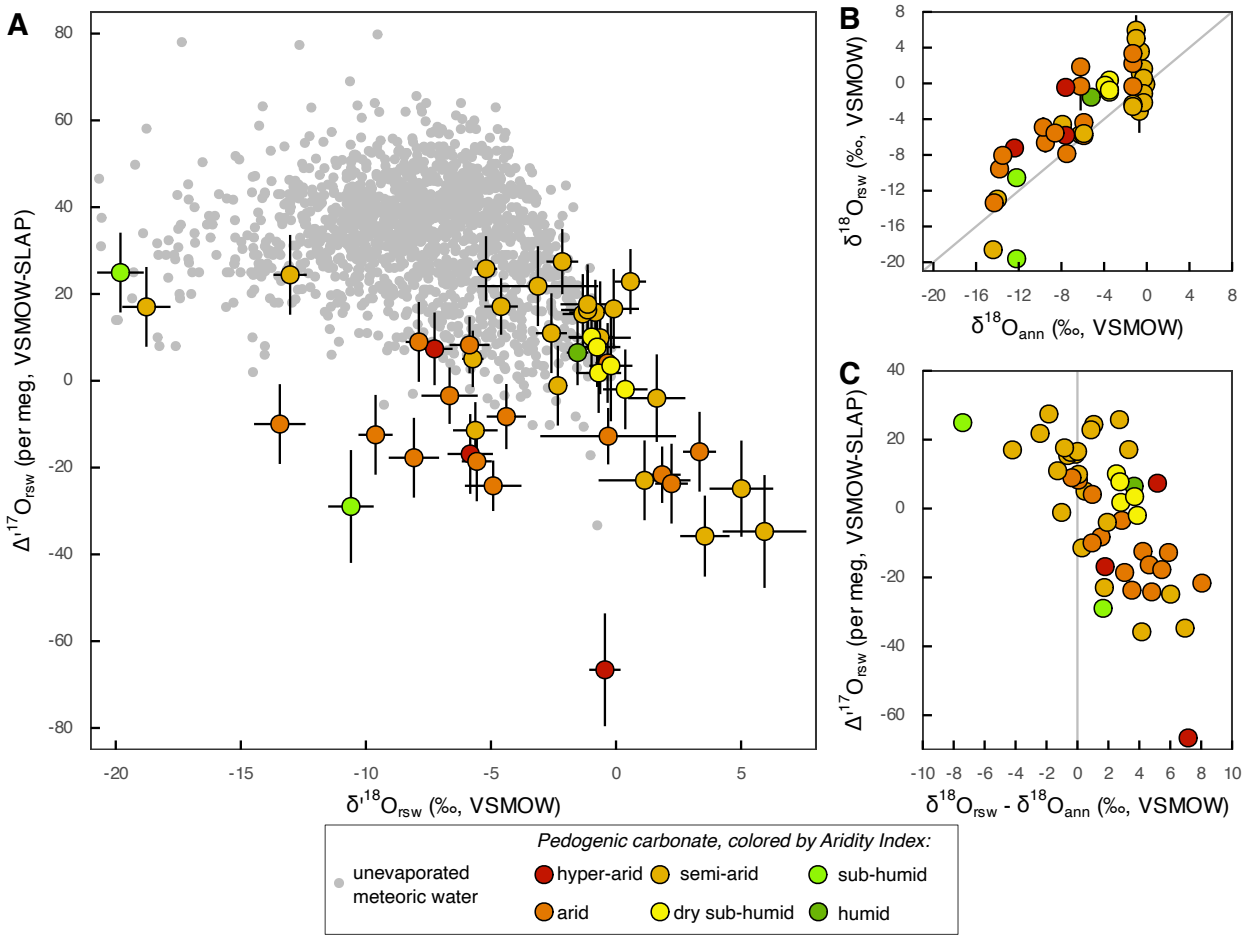

Figure 4. Triple oxygen isotopes of soil waters reconstructed from pedogenic carbonate and of global meteoric waters. A) Data from all pedogenic carbonate samples ($\Delta'^{17}O_{rsw}$ and $\delta^{18}O_{rsw}$) (colored dots) and global unevaporated meteoric waters (gray dots). This figure shows data from all soil depths, unlike Figure 5 which is restricted to depths > 30 cm. The global meteoric water data were compiled by Aron et al. (2021) and have been filtered to include only 'unevaporated' waters: tap, spring, river or stream, precipitation, and groundwater. **B)** Mean annual $\delta^{18}O$ values of precipitation ($\delta^{18}O_{ann}$) and $\delta^{18}O_{rsw}$ values calculated from pedogenic carbonates in this study. The gray line is the 1:1 line. $\delta^{18}O_{ann}$ is from the OIPC or GNIP (see methods in Section 2.1). **C)** The difference between $\delta^{18}O_{rsw}$ and $\delta^{18}O_{ann}$ in ‰ and its correlation to $\Delta'^{17}O_{rsw}$. The vertical line indicates a $\delta^{18}O_{rsw}$ -$\delta^{18}O_{ann}$ difference of 0 ‰, equivalent to the 1:1 line in panel B.

1602

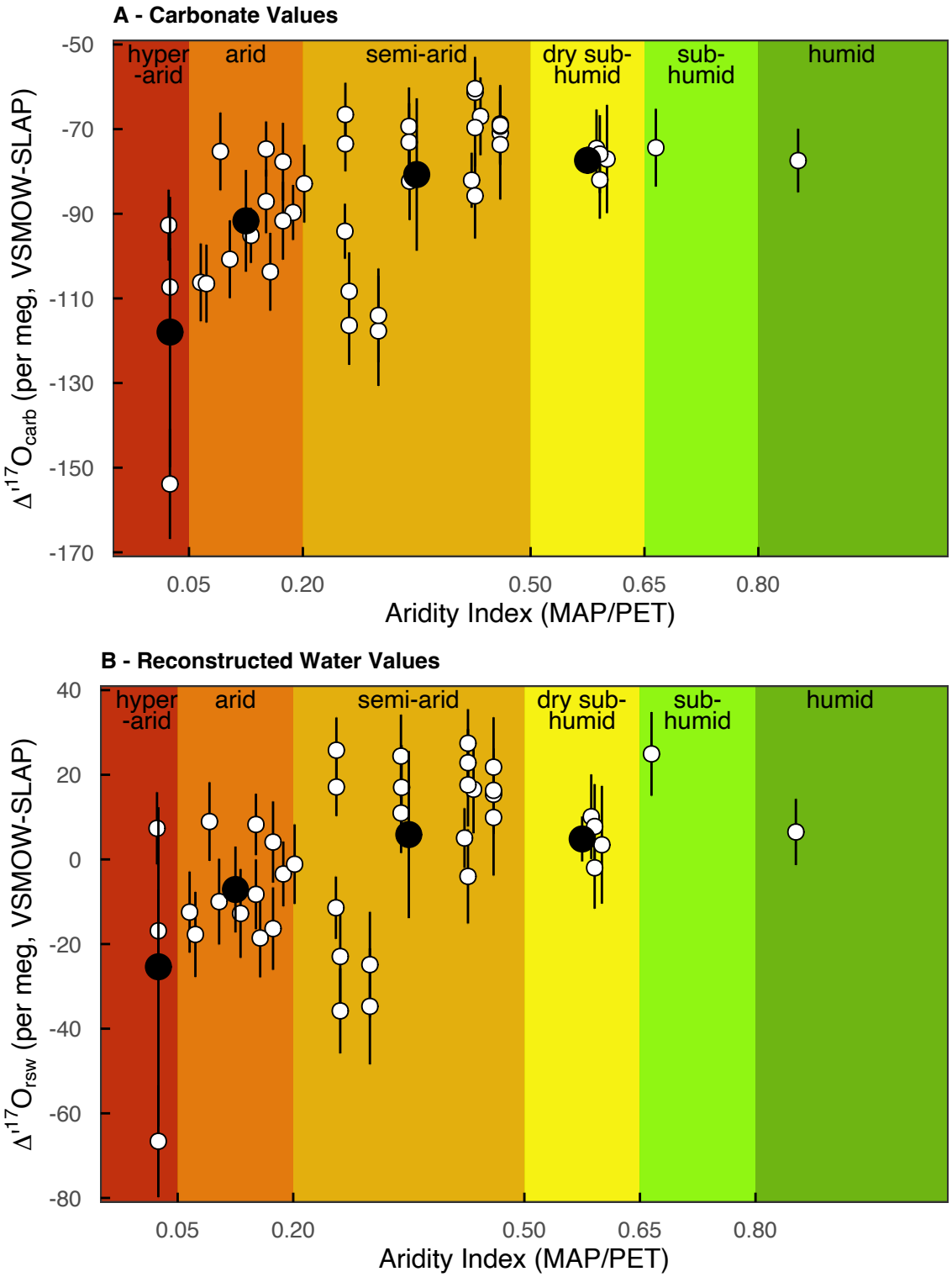
A - Carbonate Values
hyper -arid
arid
semi-arid
dry sub-humid
sub-humid
humid
-50
-70
-90
-110
-130
-150
-170
0.05
0.20
0.50
0.65
0.80
Aridity Index (MAP/PET)
Δ'17Ocarb (per meg, VSMOW-SLAP)
B - Reconstructed Water Values
40
20
0
-20
-40
-60
-80
Δ'17Orsw (per meg, VSMOW-SLAP)

1603

Figure 5: Triple oxygen isotope composition of pedogenic carbonate vs aridity. A) Results presented for carbonate mineral, $\Delta'^{17}O_{carb.}$ **B)** Results presented as $\Delta'^{17}O_{rsw}$ values, which are calculated from $\Delta'^{17}O_{carb}$, λ_{cc-w} = 0.5250, and mineral growth temperatures (based on Δ_{47} for all but four samples, see Table 3). Samples that are <30 cm in depth are not shown. Error bars are external errors propagated from 1 S.E. of replicates and uncertainty in the mineral-water fractionation. Small white dots indicate individual pedogenic carbonate samples (each with 1–4 replicate measurements). Large black dots show the mean $\Delta'^{17}O$ value for each AI class, the error is 1 S.D. (no mean shown for the sub-humid and humid classes that each have one sample).

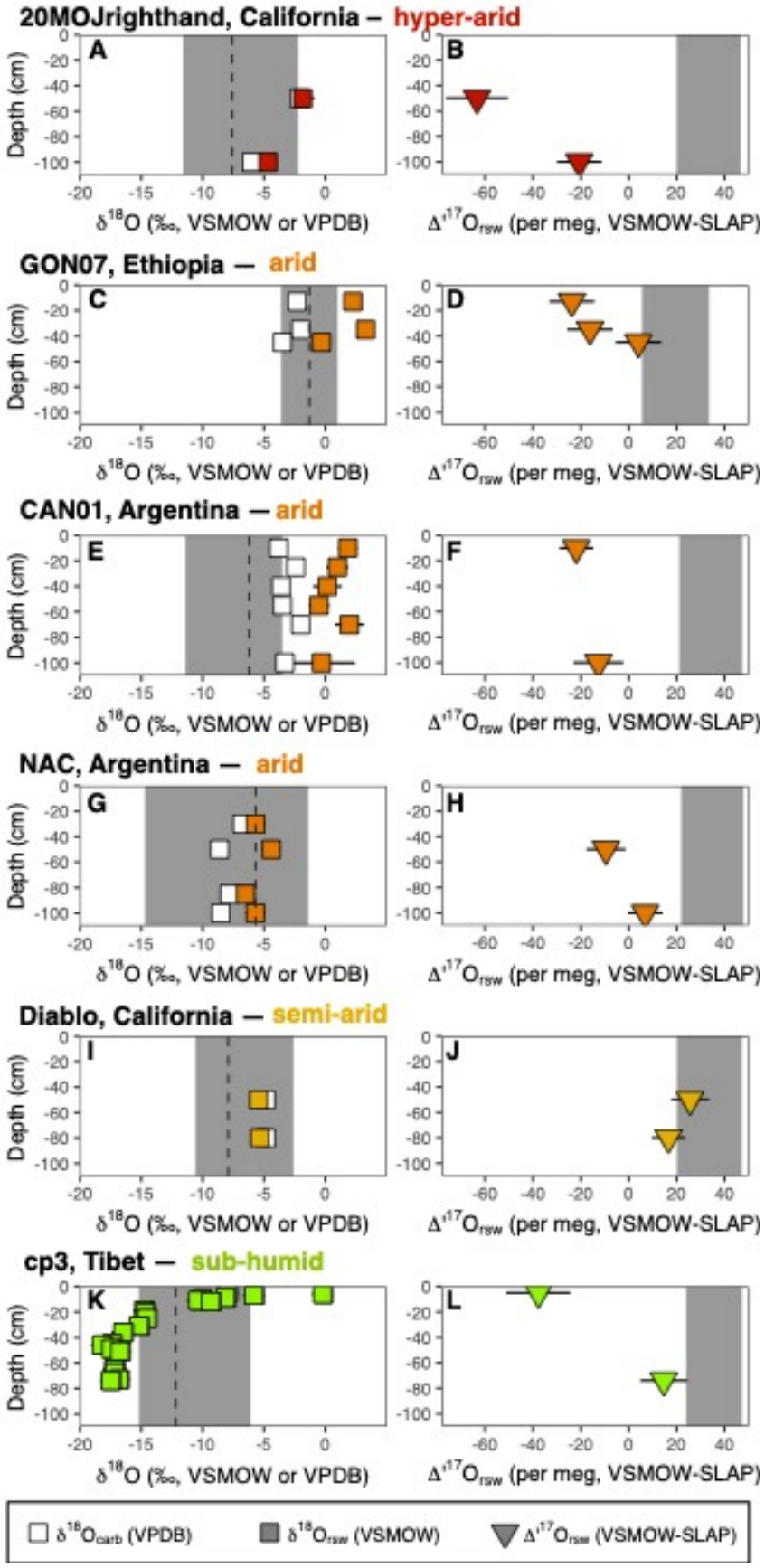
20MOJrighthand, California – hyper-arid
A
B
GON07, Ethiopia — arid
C
D
CAN01, Argentina — arid
E
F
NAC, Argentina — arid
G
H
Diablo, California — semi-arid
I
J
cp3, Tibet — sub-humid
K
L
Depth (cm)
δ18O (‰, VSMOW or VPDB)
Δ'17Orsw (per meg, VSMOW-SLAP)
δ18Ocarb (VPDB)
δ18Orsw (VSMOW)
Δ'17Orsw (VSMOW-SLAP)

1613

Figure 6: Stable isotope depth profiles for soil sites with measurements at multiple depths. Reconstructed water values ($\delta^{18}O_{rsw}$, $\Delta'^{17}O_{rsw}$) are colored by aridity and $\delta^{18}O_{carb}$ is in white. **Left Panels (A, C, E, G, I, K)** show $\delta^{18}O_{carb}$ and $\delta^{18}O_{rsw}$. Gray shading indicates the possible range of $\delta^{18}O$ of precipitation at each site. The dashed vertical line is mean annual $\delta^{18}O$ of precipitation weighted by amount ($\delta^{18}O_{ann}$), derived from the OIPC or GNIP (Section 2.3). Error bars for $\delta^{18}O_{rsw}$ are propagated error from the Δ_{47} temperature and error in $\delta^{18}O_{carb}$; if they are not visible, they are smaller than the symbol. **Right Panels (B, D, F, H, J, L)** show $\Delta'^{17}O_{rsw}$. The gray rectangle shows a likely range of $\Delta'^{17}O_{mw}$ that is estimated using the mean of $\Delta'^{17}O$ values of global, unevaporated meteoric waters within the range of precipitation $\delta^{18}O$ values at each site (water data from Aron et al., 2021, as in Figure 4).

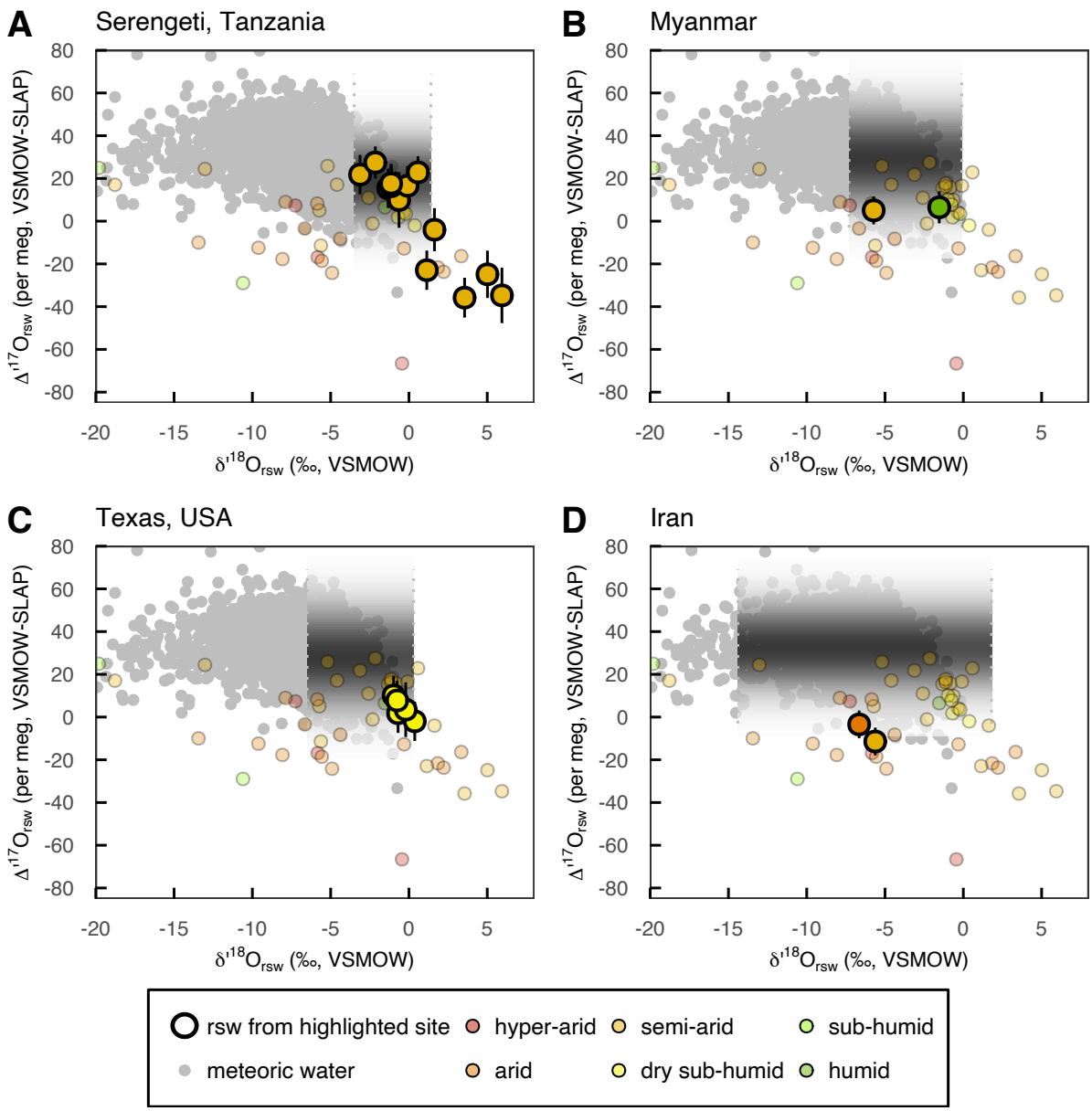

1624

1625 **Figure 7: Triple oxygen isotope compositions of geographically related samples.**

The reconstructed water values from pedogenic carbonate samples of interest are shown as large dots with thick outline. All other pedogenic carbonate samples are shown for context (colored dots, same as Figure 4). Unevaporated global meteoric waters are also shown for context (gray dots, same as Figure 4). The typical isotopic composition of precipitation in each region is illustrated with the faded gray rectangles. The width of the rectangle is determined by the range in precipitation $\delta^{18}O$ at each site. The darkness of the shading of the rectangle illustrates the likelihood of a $\Delta'^{17}O$ value, as determined by the Gaussian distribution of the $\Delta'^{17}O$ values of the global meteoric water data within the range of $\delta^{18}O$ values at that site.

Table 1: Location and climate information for pedogenic carbonates in this study

Sample Name	Depth (cm)	Latitude[a]	Longitude	Elev-ation (m)	Location	Relevant publications	MAAT °C [b]	MAP (mm/year)[b]	PET (mm/year)[b]	Aridity Index (MAP/PET)[b]	$\delta^{18}O_{ann}$[c]
GONJQ-305-1	50	11.1481	40.3357	694	Afar, Ethiopia	Passey et al. 2014 ($\Delta'^{17}O$); Passey et al. 2010 (Δ_{47})	26	461	2284	0.2018	-1.3
GON07-4.3.1	13	11.1653	40.4950	637	Afar, Ethiopia	Passey et al. 2014 ($\Delta'^{17}O$); Passey et al. 2010 (Δ_{47})	27	403	2318	0.1738	-1.3
GON07-4.6.2	35	11.1653	40.4950	637	Afar, Ethiopia	Passey et al. 2014 ($\Delta'^{17}O$); Passey et al. 2010 (Δ_{47})	27	403	2318	0.1738	-1.3
GON07-4.7.1	45	11.1653	40.4950	637	Afar, Ethiopia	Passey et al. 2014 ($\Delta'^{17}O$); Passey et al. 2010 (Δ_{47})	27	403	2318	0.1738	-1.3
CN2008-DM-164-130-1	130	42.0153	111.5743	1306	Inner Mongolia	Passey et al. 2014 ($\Delta'^{17}O$); Passey et al. 2010 (Δ_{47})	4	227	1444	0.1571	-8.6
CA08-005-1	140	34.4212	-116.7890	982	California, USA	Passey et al. 2014 ($\Delta'^{17}O$); Passey et al. 2010 (Δ_{47})	17	238	2604	0.0913	-7.5
ET05-AWSH-48-1	130	8.7884	39.6617	1259	Afar, Ethiopia	Passey et al. 2014 ($\Delta'^{17}O$); Passey et al. 2010 (Δ_{47})	23	726	2134	0.34	-1.3
BUR MH 30 Buff	30	30.4909	-96.4677	70	Texas, USA	Ji 2016 ($\Delta'^{17}O$)	20	1010	1721	0.5868	-3.5
SHP 80 XTLN	80	30.6174	-96.3000	90	Texas, USA	Ji 2016 ($\Delta'^{17}O$)	20	1022	1728	0.5912	-3.5
RCWMA LD 129-140E	130	31.9458	-96.0563	90	Texas, USA	Ji 2016 ($\Delta'17O$); Michel et al., 2013	19	1015	1689	0.6006	-3.9
BUR MH 70 White	70	30.4909	-96.4677	70	Texas, USA	Ji 2016 ($\Delta'^{17}O$)	20	1010	1721	0.5868	-3.5
SHP 100 Buff	100	30.6174	-96.3000	90	Texas, USA	Ji 2016 ($\Delta'^{17}O$); Robinson et al., 2002	20	1022	1728	0.5912	-3.5
CAN01-10	10	-32.5919	-68.9053	1000	Mendoza, Argentina	Ringham et al., 2016 (Δ_{47})	16	245	1861	0.1316	-6.2

CAN01-100	100	-32.5919	-68.9053	1000	Mendoza, Argentina	Ringham et al., 2016 (Δ_{47})	16	245	1861	0.1316	-6.2
NAC-50	50	-34.0500	-67.9028	600	Mendoza, Argentina	Ringham et al., 2016 (Δ_{47})	16	271	1787	0.1516	-5.9
NAC-100	100	-34.0500	-67.9028	600	Mendoza, Argentina	Ringham et al., 2016 (Δ_{47})	16	271	1787	0.1516	-5.9
Diablo 50	50	37.7397	-121.8370	180	California, USA	this work	15	442	1726	0.256	-7.9
Diablo 80	80	37.7397	-121.8370	180	California, USA	this work	15	442	1726	0.256	-7.9
LH2-40	40	39.4373	-119.0663	1274	Nevada, USA	this work	12	131	1998	0.0655	-13.8
Loyalton2-40	40	39.6631	-120.3155	1500	California, USA	this work	9	565	1662	0.3398	-14
20MOJ-righthand-100	100	35.1914	-116.1401	380	California, USA	this work	22	79	3162	0.0249	-7.6
20MOJ-righthand-50	50	35.1914	-116.1401	380	California, USA	this work	22	79	3162	0.0249	-7.6
TB1701	50	36.9088	48.8046	2190	Zanjan Province, Iran	this work; Paolo Ballato pers. Comm	14	371	1452	0.2554	-5.9
AN1702	110	36.9124	47.4441	695	Zanjan Province, Iran	this work; Paolo Ballato pers. Comm	11	305	1629	0.1871	-9.5
19NOD04	90	22.8508	94.3559	120	Myanmar	Licht et al., 2022 (Δ_{47})	25	1414	1658	0.8524	-5.2
20ND03	170	21.4107	94.7243	300	Myanmar	Licht et al., 2022 (Δ_{47})	26	751	1778	0.4223	-6.2
NM140809-1B	NA	36.3567	-105.7338	2053	New Mexico, USA	Hudson et al., in prep (Δ_{47})	9	295	1770	0.1666	-9.7
PDJ 4055 115a	115	-22.9386	-67.9482	4055	Atacama Desert, Chile	Quade et al., 2007	9	49	2104	0.0232	-12.4
cp3 5-7	5	28.2850	87.3847	3741	Tibet	Breecker 2008	6	893	1342	0.665	-12.2
cp3 65-68	65	28.2850	87.3847	3741	Tibet	Breecker 2008	6	893	1342	0.665	-12.2
cp4-75	75	28.2556	87.0838	4825	Tibet	Breecker 2008	0	385	1130	0.3406	-14.4
FLV-Site-B-84-94cm	84 to 94	37.8812	-118.1804	1745	Nevada, USA	Oerter & Amundson 2016	11	156	2136	0.073	-13.5

FLV-Site-C-74-100cm	74 to 100	37.8554	-118.2301	2140	Nevada, USA	Oerter & Amundson 2016	8	204	1965	0.1038	-14.3
18-SS-215A	80	-2.9603	35.4363	1354	Serengeti, Tanzania	Beverly et al., 2021 ($\Delta'^{17}O$)	21	499	1911	0.261	-0.6
18-SS-215(D-G)	80	-2.9603	35.4363	1354	Serengeti, Tanzania	Beverly et al., 2021 ($\Delta'^{17}O$)	21	499	1911	0.261	-0.6
18-SS-235	50	-2.9355	35.2473	1549	Serengeti, Tanzania	Beverly et al., 2021 ($\Delta'^{17}O$)	20	558	1862	0.2995	-1
18-SS-236(A-C)	50	-2.9355	35.2473	1549	Serengeti, Tanzania	Beverly et al., 2021 ($\Delta'^{17}O$)	20	558	1862	0.2995	-1
18-SS-69A	60	-2.6169	34.8966	1637	Serengeti, Tanzania	Beverly et al., 2021 ($\Delta'^{17}O$)	19	805	1749	0.46	-0.7
18-SS-70A	80	-2.6169	34.8966	1637	Serengeti, Tanzania	Beverly et al., 2021 ($\Delta'^{17}O$)	19	805	1749	0.46	-0.7
18-SS-71A	100	-2.6169	34.8966	1637	Serengeti, Tanzania	Beverly et al., 2021 ($\Delta'^{17}O$)	19	805	1749	0.46	-0.7
18-SS-72B	120	-2.6169	34.8966	1637	Serengeti, Tanzania	Beverly et al., 2021 ($\Delta'^{17}O$)	19	805	1749	0.46	-0.7
18-SS-73B	140	-2.6169	34.8966	1637	Serengeti, Tanzania	Beverly et al., 2021 ($\Delta'^{17}O$)	19	805	1749	0.46	-0.7
18-SS-49A	60	-2.3290	34.8478	1425	Serengeti, Tanzania	Beverly et al., 2021 ($\Delta'^{17}O$)	21	819	1886	0.434	-0.1
18-SS-78B	70	-2.1654	33.9734	1153	Serengeti, Tanzania	Beverly et al., 2021 ($\Delta'^{17}O$)	23	846	1982	0.4268	-0.3
18-SS-79A	90	-2.1654	33.9734	1153	Serengeti, Tanzania	Beverly et al., 2021 ($\Delta'^{17}O$)	23	846	1982	0.4268	-0.3
18-SS-80B	100	-2.1654	33.9734	1153	Serengeti, Tanzania	Beverly et al., 2021 ($\Delta'^{17}O$)	23	846	1982	0.4268	-0.3
18-SS-81A	130	-2.1654	33.9734	1153	Serengeti, Tanzania	Beverly et al., 2021 ($\Delta'^{17}O$)	23	846	1982	0.4268	-0.3

[a] Datum WGS 1984.

[b] MAAT is Mean Annual Air Temperature, MAP is Mean Annual Precipitation, PET is potential evapotranspiration. All climate data are from World Clim 2 and Version 3 of the Global Aridity Index and Potential Evapotranspiration Database (30 arc-second grid resolution) (Fick and Hijmans, 2017; Zomer et al., 2022)

[c] Annual weighted mean of precipitation $\delta^{18}O$ from the Oxygen Isotopes in Precipitation Calculator (OIPC) (Bowen and Revenaugh, 2003), except for samples from Ethiopia and NAC samples from Argentina where values from the Global Network of Isotopes in Precipitation values are used instead (see text 2.3).

1644

1645 **Table 2:** Triple oxygen isotope data (average values) for pedogenic carbonate samples
1646

Sample Name	number of analyses via O_2	$\delta'^{17}O_{carb} \pm 1\sigma$ ($O_2/CaCO_3$) (‰, VSMOW-SLAP)	$\delta'^{18}O_{carb} \pm 1\sigma$ ($O_2/CaCO_3$) (‰, VSMOW-SLAP)	$\Delta'^{17}O_{carb} \pm$ ERR ($O_2/CaCO_3$) (per meg, VSMOW-SLAP)[a]	$\Delta'^{17}O_{rsw} \pm$ ERR [3] ($O_2/CaCO_3$) (per meg, VSMOW-SLAP)[b]	$\delta'^{18}O_{rsw} \pm$ ERR (‰, VSMOW)[c]	Reference for $\Delta'^{17}O$ values [d]
GONJQ-305-1	2	13.078 ± 0.086	24.927 ± 0.168	-83 ± 9	-1 ± 9	-2 ± 0	Passey et al. (2014)
GON07-4.3-1	2	14.756 ± 0.428	28.139 ± 0.817	-101 ± 9	-24 ± 10	2 ± 1	Passey et al. (2014)
G0N07-4.6 -2	2	14.925 ± 0.008	28.44 ± 0.02	-92 ± 9	-16 ± 10	3 ± 1	Passey et al. (2014)
G0N07-4.7 -1	2	14.144 ± 0.268	26.936 ± 0.511	-78 ± 9	4 ± 10	0 ± 0	Passey et al. (2014)
CN2008 -DM -164-130 -1	2	11.941 ± 0.962	22.813 ± 1.824	-104 ± 9	-19 ± 10	-6 ± 1	Passey et al. (2014)
CA08-005-1	2	10.585 ± 0.199	20.19 ± 0.368	-75 ± 9	9 ± 9	-8 ± 1	Passey et al. (2014)
ET05-AWSH-48-1	2	13.354 ± 0.106	25.429 ± 0.182	-73 ± 9	11 ± 10	-3 ± 1	Passey et al. (2014)
BUR MH 30Buff	2	14.299 ± 1.127	27.237 ± 2.135	-82 ± 9	2 ± 9	-1 ± 1	Ji (2016)
SHP 80 XTLN	2	14.193 ± 0.072	27.036 ± 0.142	-82 ± 9	-2 ± 10	0 ± 1	Ji (2016)
RCWMA LD 129-140E	2	13.986 ± 0.251	26.635 ± 0.442	-77 ± 13	3 ± 13	0 ± 1	Ji (2016)
BUR MH 70 White	2	14.306 ± 0.43	27.237 ± 0.823	-75 ± 9	10 ± 10	-1 ± 1	Ji (2016)
SHP 100 Buff	2	14.252 ± 0.522	27.136 ± 0.99	-76 ± 9	8 ± 10	-1 ± 1	Ji (2016)
CAN01 -10	4	13.967 ± 0.268	26.635 ± 0.508	-96 ± 7	-22 ± 7	2 ± 1	this work
CAN01 -100	4	14.233 ± 0.593	27.136 ± 1.122	-95 ± 7	-13 ± 11	0 ± 3	this work
NAC-50	3	11.474 ± 0.56	21.895 ± 1.065	-87 ± 8	-8 ± 8	-4 ± 1	this work
NAC-100	4	11.433 ± 0.165	21.795 ± 0.292	-75 ± 7	8 ± 7	-6 ± 1	this work
Diablo 50	3	13.445 ± 0.487	25.59 ± 0.918	-67 ± 8	26 ± 8	-5 ± 0	this work
Diablo 80	4	13.443 ± 0.768	25.6 ± 1.445	-73 ± 7	17 ± 7	-5 ± 1	this work
LH2-40	2	11.321 ± 0.034	21.643 ± 0.067	-106 ± 9	-12 ± 9	-10 ± 1	this work
Loyalton2-40	2	9.555 ± 0.291	18.228 ± 0.56	-69 ± 9	24 ± 10	-13 ± 1	this work
MOJ-righthand-100	1	14.968 ± NA	28.64 ± NA	-154 ± 13	-67 ± 14	0 ± 1	this work
MOJ-righthand-50	2	12.735 ± 0.009	24.323 ± 0.019	-107 ± 9	-17 ± 10	-6 ± 1	this work
TB1701	4	11.493 ± 0.498	21.946 ± 0.942	-94 ± 7	-11 ± 7	-6 ± 1	this work

AN1702	4	11.578 ± 0.485	22.097 ± 0.915	-90 ± 7	-3 ± 8	-7 ± 1	this work
19ND04	3	13.88 ± 0.098	26.434 ± 0.167	-77 ± 8	6 ± 8	-2 ± 0	this work
20ND03	4	12.229 ± 0.459	23.317 ± 0.854	-82 ± 7	5 ± 7	-6 ± 0	this work
NM140809-1B	5	12.762 ± 0.632	24.384 ± 1.181	-112 ± 6	-24 ± 7	-5 ± 1	this work
PDJ 4055 115a	3	13.684 ± 0.496	26.092 ± 0.952	-93 ± 8	7 ± 9	-7 ± 1	this work
cp3 5-7	1	11.757 ± NA	22.511 ± NA	-128 ± 13	-29 ± 14	-11 ± 1	this work
cp3 65-68	2	6.946 ± 0.184	13.296 ± 0.34	-74 ± 9	25 ± 10	-20 ± 1	this work
cp4 75	2	7.485 ± 0.326	14.333 ± 0.61	-82 ± 9	17 ± 10	-19 ± 1	this work
FLV-Site-B-84-94cm	2	11.252 ± 0.105	21.512 ± 0.182	-107 ± 9	-18 ± 10	-8 ± 1	this work
FLV-Site-C-74-100cm	2	8.78 ± 0.081	16.82 ± 0.167	-101 ± 9	-10 ± 10	-13 ± 1	this work
18-SS-215A	2	15.521 ± 1.179	29.602 ± 2.227	-108 ± 9	-23 ± 11	1 ± 2	Beverly et al. (2021)
18-SS-215(D-G)	3	15.941 ± 0.691	30.412 ± 1.338	-116 ± 9	-36 ± 10	4 ± 1	Beverly et al. (2021)
18-SS-235	1	17.616 ± NA	33.587 ± NA	-118 ± 13	-35 ± 14	6 ± 2	Beverly et al. (2021)
18-SS-236(A-C)	4	18.225 ± 0.408	34.733 ± 0.777	-114 ± 11	-25 ± 12	5 ± 1	Beverly et al. (2021)
18-SS-69A	3	14.739 ± 0.623	28.049 ± 1.176	-71 ± 8	16 ± 9	-1 ± 1	Beverly et al. (2021)
18-SS-70A	2	14.042 ± 0.700	26.725 ± 1.329	-69 ± 9	15 ± 10	-1 ± 1	Beverly et al. (2021)
18-SS-71A	2	14.317 ± 0.776	27.247 ± 1.49	-69 ± 9	22 ± 12	-3 ± 2	Beverly et al. (2021)
18-SS-72B	1	14.297 ± NA	27.217 ± NA	-74 ± 13	10 ± 14	-1 ± 1	Beverly et al. (2021)
18-SS-73B	2	14.36 ± 0.325	27.327 ± 0.623	-69 ± 9	16 ± 10	-1 ± 1	Beverly et al. (2021)
18-SS-49A	2	14.589 ± 0.353	27.758 ± 0.676	-67 ± 9	17 ± 9	0 ± 1	Beverly et al. (2021)
18-SS-78B	3	15.163 ± 0.057	28.881 ± 0.079	-86 ± 10	-4 ± 11	2 ± 1	Beverly et al. (2021)
18-SS-79A	3	15.055 ± 0.299	28.63 ± 0.547	-61 ± 8	23 ± 8	1 ± 1	Beverly et al. (2021)
18-SS-80B	2	14.687 ± 0.210	27.949 ± 0.394	-70 ± 9	18 ± 10	-1 ± 1	Beverly et al. (2021)
18-SS-81A	3	14.273 ± 0.710	27.146 ± 1.351	-60 ± 8	27 ± 8	-2 ± 1	Beverly et al. (2021)

[a] $\Delta'^{17}O$ is reported as a carbonate mineral value (i.e., $O_2/CaCO_3$, normalized to IAEA 603 and IAEA C1 = -100 per meg (Wostbrock et al., 2020) and calculated using $\lambda_{ref} = 0.528$. $\Delta'^{17}O$ ERR of the carbonate mineral value is 1 standard error (S.E.). S.E. is calculated using whichever is larger, the standard deviation of the sample replicate values or the long-term standard deviation of the carbonate standard 102GCAZ01 (13 per meg).

[b] $\Delta'^{17}O$ of water reconstructed from carbonate. Calculated using $\lambda_{ref} = 0.528$ and the carbonate-water triple oxygen isotope exponent value of $\lambda_{cc\ -w} = 0.5250$. Error in the $\Delta'^{17}O_{rsw}$ values is calculated using the external error in the $\Delta'^{17}O_{carb}$ value, external error in the growth temperature estimate, and uncertainty in the carbonate-water fractionation factors. Error is calculated with Monte Carlo resampling.

[c] Reconstructed $\delta^{18}O$ values are calculated using the $\delta^{18}O$ of carbonate measured via CO_2 which can be found in Table 3. Error is calculated with Monte Carlo resampling considering external error in the growth temperature estimate and uncertainty in the carbonate-water fractionation factors.

[d] Samples originally reported in Beverly et al. (2021), Passey et al. (2014), and Ji (2016) are recalculated in this study to report the values as carbonate mineral values via Wostbrock et al. (2020).

1663 **Table 3:** Clumped isotope data and alternate growth temperature data for pedogenic carbonate samples
1664

Sample Name	number of analyses via CO_2	$\delta^{13}C$ (‰, VPDB)	$\delta^{18}O$ (via CO2) (‰, VPDB)	Δ_{47} ICDES25 ± ERR (‰)[a]	$T\Delta_{47}$ ± ERR °C	Other Growth Temp.	Reference for Δ_{47}/Temp.
GONJQ-305-1	2	-2.5	-5.5	0.628 ± 0.008	29 ± 1.8	-	Passey et al. (2010)
GON07-4.3.1	1	-0.2	-2.3	0.600 ± 0.013	35.9 ± 3.4	-	Passey et al. (2010)
GON07-4.6.2	1	-2.9	-2.0	0.582 ± 0.013	40.3 ± 3.5	-	Passey et al. (2010)
GON07-4.7.1	2	-1.5	-3.5	0.629 ± 0.009	28.9 ± 2.4	-	Passey et al. (2010)
CN2008-DM-164-130-1	1	-3.0	-7.6	0.653 ± 0.013	23.4 ± 3	-	Passey et al. (2010)
CA08-005-1	2	-3.4	-10.2	0.646 ± 0.009	24.9 ± 2.5	-	Passey et al. (2010)
ET05-AWSH-48-1	1	0.5	-5.0	0.645 ± 0.013	25.2 ± 3.1	-	Passey et al. (2010)
BUR MH 30 Buff	1	-3.4	-3.2	0.69 ± 0.013	25.6 ± 4.5	-	Ji (2016)
SHP 80 XTLN	1	-10.5	-3.4	0.671 ± 0.013	32 ± 4.5	-	Ji (2016)
RCWMA LD 129-140E	1	-3.9	-3.8	0.674 ± 0.013	31.1 ± 4.5	-	Ji (2016)
BUR MH 70 White	1	-2.4	-3.2	0.694 ± 0.013	24.2 ± 4.5	-	Ji (2016)
SHP 100 Buff	1	-10.1	-3.3	0.688 ± 0.013	25.8 ± 4.5	-	Ji (2016)
CAN01-10	3	-1.88	-3.80	0.646 ± 0.011	42 ± 4.1	-	Ringham et al. (2016), reprocessed in Kelson et al. (2020)
CAN01-100	3	-2.66	-3.30	0.687 ± 0.045	28 ± 13.7	-	Ringham et al. (2016), reprocessed in Kelson et al. (2020)
NAC-50	4	-5.83	-8.61	0.668 ± 0.012	34 ± 4.1	-	Ringham et al. (2016), reprocessed in Kelson et al. (2020)
NAC-100	2	-5.51	-8.51	0.69 ± 0.013	27 ± 4.1	-	Ringham et al. (2016), reprocessed in Kelson et al. (2020)
Diablo 50	3	-8.91	-4.84	0.724 ± 0.008	11.7 ± 2.2	-	this work; SCIPP at UM
Diablo 80	2	-9.91	-4.83	0.713 ± 0.01	15 ± 2.8	-	this work; SCIPP at UM
LH2-40	3	-3.19	-8.76	0.724 ± 0.008	11.7 ± 2.5	-	this work; IPL lab at UM
Loyalton2-40	4	-8.41	-12.14	0.728 ± 0.011	10.6 ± 3.3	-	this work; IPL lab at UM
20MOJ-righthand-50	1	-2.35	-1.80	0.712 ± 0.013	15.3 ± 4	-	this work; SCIPP at UM
20MOJ-righthand-100	2	-3.94	-6.10	0.696 ± 0.009	20.4 ± 3	-	this work; SCIPP at UM
TB1701	-	-7.21	-8.46	-	-	27.4 ± 4.5	Mean warm quarter air temperature (Jun, Jul, Aug, Sep) from Takab climate station; Islamic

							Republic of Iran Meteorological Organization
AN1702	-	-6.95	-8.31	-	-	21.6 ± 5.5	Mean warm quarter air temperature (Jun, Jul, Aug, Sep) from Abbar climate station
19NOD04	4	-13.9	-4.0	0.68 ± 0.007	25.7 ± 2.2	-	Licht et al. (2022) (SCIPP at UM)
20ND03	4	-9.2	-7.1	0.696 ± 0.007	20.5 ± 2.3	-	Licht et al. (2022) (SCIPP at UM)
NM140809-1B	-	-3.17	-6.04	-	-	19.5	Mean warm quarter air temperature from NOAA climate normals in Taos (USC00298668)
PDJ 4055 115a	2	-3.63	-4.34	0.761 ± 0.01	1 ± 2.6	-	this work; IPL lab at UM
cp3 5-7	-	0.55	-7.9	-	-	2.3 ± 2.8	Δ47-Temp from cp4
cp3 65-68	-	1.5	-17	-	-	2.3 ± 2.8	Δ47-Temp from cp4
cp4-75	4	-6.78	-17.39	0.758 ± 0.011	2.3 ± 2.8		this work; IPL lab at UM
FLV-Site-B-84-94cm	-	-2.72	-8.89	-	-	17.6 ± 5	average of soil temperatures measured in May, August, and April
FLV-Site-C-74-100cm	-	-2.71	-13.53	-	-	14.5 ± 5	average of soil temperatures measured in May, Aug., and Apr.
18-SS-215A	4	-0.07	-0.84	0.69 ± 0.028	23 ± 9	-	Beverly et al. (2021)
18-SS-215(D-G)	2	2.12	-0.03	0.665 ± 0.002	31 ± 4.9	-	Beverly et al. (2021)
18-SS-235	5	1.89	3.15	0.677 ± 0.024	27 ± 8	-	Beverly et al. (2021)
18-SS-236(A-C)	5	1.75	4.3	0.708 ± 0.02	17 ± 6	-	Beverly et al. (2021)
18-SS-69A	3	0.91	-2.39	0.694 ± 0.008	21 ± 5.2	-	Beverly et al. (2021)
18-SS-70A	2	1.16	-3.71	0.685 ± 0.002	25 ± 4.1	-	Beverly et al. (2021)
18-SS-71A	4	0.83	-3.19	0.718 ± 0.017	14 ± 10.7	-	Beverly et al. (2021)
18-SS-72B	3	0.94	-3.22	0.68 ± 0.011	26 ± 6.5	-	Beverly et al. (2021)
18-SS-73B	3	1.22	-3.11	0.689 ± 0.008	23 ± 4.8	-	Beverly et al. (2021)
18-SS-49A	2	0.66	-2.68	0.68 ± 0.002	26 ± 4.8	-	Beverly et al. (2021)
18-SS-78B	3	1.47	-1.56	0.669 ± 0.01	29 ± 5.5	-	Beverly et al. (2021)
18-SS-79A	3	1.02	-1.81	0.684 ± 0.011	25 ± 3.2	-	Beverly et al. (2021)
18-SS-80B	3	1.12	-2.49	0.699 ± 0.014	20 ± 4.7	-	Beverly et al. (2021)
18-SS-81A	3	0.37	-3.29	0.703 ± 0.011	19 ± 3.2	-	Beverly et al. (2021)

[a]All Δ_{47} values are corrected to acid digestion at 25 °C. Data new to this work (the SCIPP lab and IPL) are in the ICDES-25 framework and temperature was calculated using the calibration of Anderson et al. (2021) (note: the Anderson calibration is reported in ICDES-90; the intercept must be adjusted with an acid

fractionation factor (i.e., 0.088) to calculate temperatures from ICDES-25 values). Data from Passey et al. (2010) are reported in the 'HG' reference frame of Caltech. Samples were reacted at 90°C and corrected with an acid fractionation factor of 0.081. Mineral growth temperatures were calculated using the calibration of Ghosh et al. (2006). Samples from Ji (2016) are in the CDES of Dennis et al. (2011) and temperatures were calculated with Equation 5 from Passey and Henkes (2012). The samples were reacted in acid held at 90 °C and are corrected with an acid fractionation factor of 0.082 (Delfiese et al., 2015). The samples from Beverly et al. (2021) are reported in the CDES of Dennis et al. (2011) (using gas standards). Raw Δ_{47} values were corrected with the ^{17}O correction parameters of Brand et al. (2010). Samples $\Delta 47$ values were adjusted by +0.082 to correct for acid digestion at 90 °C (Defliese et al., 2015). Temperatures were calculated using the calibration of Bonifacie et al. (2017).